Molecular Cell

Technology

Ubiquiton—An inducible, linkage-specific polyubiquitylation tool

Graphical abstract

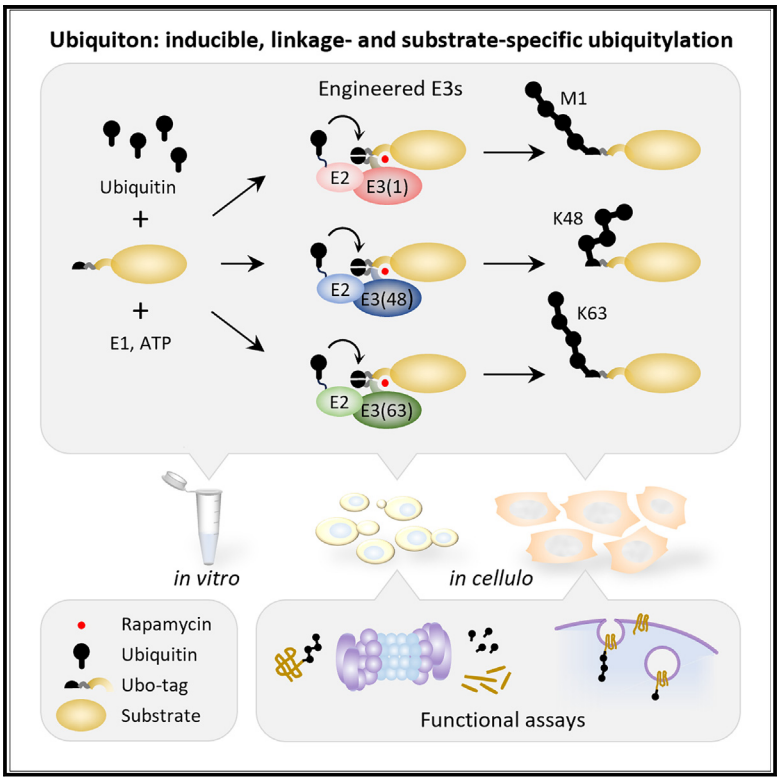

Highlights

- Ubiquiton affords inducible substrate-specific M1-, K48-, or K63-polyubiquitylation
- Ubiquiton combines custom linkage-specific E3s with cognate modification sites
- The K48-Ubiquiton acts as a rapamycin-inducible degron in yeast and human cells
- K63-polyubiquitylation is sufficient for endocytosis of a plasma membrane protein

Authors

Christian Renz, Evrydiki Asimaki, Cindy Meister, ..., Jia-Xuan Chen, Sébastien Léon, Helle D. Ulrich

Correspondence

h.ulrich@imb-mainz.de

In brief

Analytical tools for investigating ubiquitin signaling are abundant, but methods to induce linkage-specific polyubiquitylation of a protein of interest have been missing. Renz et al. have now developed rapamycin-inducible E3s specific for three major linkages and validated them for use *in vitro* in budding yeast and in mammalian cells.

Renz et al., 2024, Molecular Cell *84*, 386–400
January 18, 2024 © 2023 The Author(s). Published by Elsevier Inc.
https://doi.org/10.1016/j.molcel.2023.11.016

CellPress

CellPress
OPEN ACCESS

Molecular Cell

Technology

Ubiquiton—An inducible, linkage-specific polyubiquitylation tool

Christian Renz,[1] Evrydiki Asimaki,[1] Cindy Meister,[1] Véronique Albanèse,[2] Kirill Petriukov,[1] Nils C. Krapoth,[1] Sabrina Wegmann,[1,3] Hans-Peter Wollscheid,[1] Ronald P. Wong,[1] Amitkumar Fulzele,[1] Jia-Xuan Chen,[1] Sébastien Léon,[2] and Helle D. Ulrich[1,4,*]

[1]Institute of Molecular Biology (IMB) gGmbH, Ackermannweg 4, 55128 Mainz, Germany
[2]Université de Paris, CNRS, Institut Jacques Monod, 75013 Paris, France
[3]Present address: Merck KGaA, Frankfurter Straße 250, 64293 Darmstadt, Germany
[4]Lead contact
*Correspondence: h.ulrich@imb-mainz.de
https://doi.org/10.1016/j.molcel.2023.11.016

SUMMARY

The posttranslational modifier ubiquitin regulates most cellular processes. Its ability to form polymeric chains of distinct linkages is key to its diverse functionality. Yet, we still lack the experimental tools to induce linkage-specific polyubiquitylation of a protein of interest in cells. Here, we introduce a set of engineered ubiquitin protein ligases and matching ubiquitin acceptor tags for the rapid, inducible linear (M1-), K48-, or K63-linked polyubiquitylation of proteins in yeast and mammalian cells. By applying the so-called "Ubiquiton" system to proteasomal targeting and the endocytic pathway, we validate this tool for soluble cytoplasmic and nuclear as well as chromatin-associated and integral membrane proteins and demonstrate how it can be used to control the localization and stability of its targets. We expect that the Ubiquiton system will serve as a versatile, broadly applicable research tool to explore the signaling functions of polyubiquitin chains in many biological contexts.

INTRODUCTION

Posttranslational protein modifications add flexibility to cellular processes by reversibly modulating the properties of their targets. The highly conserved 76 amino acid protein ubiquitin is particularly versatile because it can be assembled into oligomeric structures, or "linkages," of varying topology that are thought to convey distinct biological signals.[1,2] The collective diversity of polymeric or even branched ubiquitin conjugates makes up the so-called "ubiquitin code," a complex signaling system that needs to be decoded by dedicated readers.[1,3,4] Although polyubiquitin chains linked via lysine (K) 48, K29, or K11 generally mediate targeted proteolysis by the 26S proteasome, other linkages, such as K63 or methionine (M) 1, are known for proteasome-independent signaling, for example, in the inflammatory response, intracellular vesicle transport, or DNA repair.[5–8] The linkage of a polyubiquitin chain is determined by the writers of the code, the ubiquitin-conjugating enzymes (E2s) in combination with the substrate-selective ubiquitin protein ligases (E3s).[9]

Numerous tools exist to decipher the ubiquitin code, such as antibodies, affinity probes, or proteomic methods to analyze polyubiquitin chains, and linkage-selective deubiquitylation enzymes (DUBs)[10,11] or dominant-negative ubiquitin mutants to inhibit chain formation.[12,13] Compared with these analytical and inhibitory tools, our ability to create defined ubiquitylation patterns is much more limited. Notably, it has been impossible to date to enforce the polyubiquitylation of a protein of interest with the desired linkage in cells. Being able to do so would be essential to separate the consequences of a ubiquitylation event from the signal that normally induces it. Moreover, it would allow for the targeted polyubiquitylation of proteins that are not normally subject to such modification. Finally, fundamental questions about the relevance of a given linkage for a particular biological function cannot be addressed without selectively altering the linkage of an individual ubiquitylation event—which is currently impossible due to the inherent preferences of the enzymes responsible for the modification.

One instance where inducible polyubiquitylation has been successful is the "degron" technology, where the recruitment of an endogenous E3 to a protein of interest affords polyubiquitylation and subsequent degradation by the proteasome.[14,15] This approach has been developed into proteolysis targeting chimeras (PROTACs), small molecules that act as heterobifunctional tethers or molecular glues for E3 recruitment and have started to feature in clinical applications.[16,17] However, the polyubiquitin structures resulting from such non-selective E3s are usually poorly defined or heterogeneous, affording no control over linkage or modification sites.

We have now developed an inducible, linkage-specific polyubiquitylation tool with a general substrate-targeting strategy,

 © 2023 The Author(s). Published by Elsevier Inc.
This is an open access article under the CC BY-NC license (http://creativecommons.org/licenses/by-nc/4.0/).

applicable to most cellular proteins. In analogy to the established degron systems, we named our tool the "Ubiquiton" (or "Ubo") system, as it encompasses dedicated polyubiquitylation sites on the substrates of interest but is not limited to degradative purposes. We have validated these substrate tags for M1-, K48-, and K63-selective polyubiquitylation, demonstrated their functionality in budding yeast and mammalian cells, and applied the system to control biological processes such as proteasomal degradation and ubiquitin-mediated endocytosis. Our study introduces the Ubiquiton system as a versatile research tool for the manipulation of polyubiquitin structures in cells, which promises to fill a substantial gap in our panel of methods for exploring the ubiquitin code.

DESIGN

The design of a system for the inducible, linkage-selective polyubiquitylation of any protein of interest must address the following challenges: (1) linkage selectivity of the conjugation enzymes, (2) inducible substrate selection, and (3) chain initiation. We recently engineered a set of custom E3s that fulfil the criterion of linkage selectivity, as they are derived from well-characterized domains with the intended properties:[18] the M1-specific human HOIP, which operates with several different E2s,[18,19] Cue1 from *Saccharomyces cerevisiae*, which uses the K48-specific Ubc7 as E2,[20] and budding yeast Pib1,[21] which is selective for the K63-specific E2 Ubc13·Mms2. Via fusion to a PCNA-interacting peptide (PIP), these E3s were designed to extend a pre-existing monoubiquitin unit on the replication factor proliferating cell nuclear antigen (PCNA) into a polyubiquitin chain of defined linkage. When expressed in yeast, they exhibit little or no off-target effects,[18] indicating that the second criterion, selectivity toward any substrate of choice, should be achievable by an efficient targeting system. We therefore chose a standard dimerization tool, the rapamycin (Rapa)-inducible system based on the FK506-binding protein (FKBP) and an FKBP-rapamycin-binding domain (FRB), for substrate recruitment.[22] However, the exquisite linkage specificity of these engineered "extender E3s" prevents them from chain initiation, i.e., from attaching ubiquitin to sites other than a single, specified amino group within ubiquitin itself. Stable fusion of monoubiquitin to the substrate to provide a suitable acceptor site was not an option, as it would likely trigger unexpected effects by itself or be subject to unwanted modification by cellular factors.[23] To overcome the challenge of chain initiation, we therefore made use of the split-ubiquitin technology,[24] an *in vivo* proximity sensor tool that relies on the re-folding of ubiquitin into a native-like structure from two non-interacting halves, NUb (aa 1–37) and CUb (aa 35–76) (Figure 1A). When the two halves are brought into contact via fusion to a pair of interacting proteins, ubiquitin re-assembles and is recognized and cleaved at glycine (G) 76 by cellular DUBs. We reasoned that the same principle could bring about chain initiation for our E2·E3 pairs. If the two halves of ubiquitin were supplied by the E3 and the substrate, respectively, the E3—upon recruitment to the substrate—might recognize and thus use the re-assembled ubiquitin for chain extension. In isolation, neither NUb nor CUb would be recognized as ubiquitin and would therefore remain inert. Based on the amino acid sequence of ubiquitin, the K48- and the K63-selective Ubiquiton setup would require CUb on the substrate and NUb on the enzyme, whereas the opposite arrangement would apply to all other linkages.

RESULTS

Development and feasibility of the Ubiquiton system

To test whether split ubiquitin can in principle serve as an acceptor for polyubiquitin chain extension by the engineered E3s, we used our original PCNA-specific arrangement, where a PIP mediates substrate recruitment.[18] We fused NUb to the N terminus of PIP-E3(63) and CUb, containing the ubiquitin acceptor site K63, to PCNA (Figure S1A, step 1). The resulting E3, ^{NUb}PIP-E3(63), in combination with Ubc13·Mms2, indeed afforded *in vitro* polyubiquitylation of ^{CUb}PCNA (Figure S1B). The original PIP-E3, lacking the half-ubiquitin moiety, did not polyubiquitylate ^{CUb}PCNA, indicating that activity requires reconstitution of ubiquitin from both halves. Hence, split ubiquitin can form a native-like structure on a substrate that is recognized and extended by an E3.

We then generalized the system by exchanging the PIP-mediated substrate recruitment for the Rapa-inducible FKBP·FRB dimerization system (Figure S1A, step 2). Two compatible modules were designed, based on the structure of the FKBP·Rapa·FRB complex (Figures 1B and S1C): a module consisting of NUb and the FRB domain, separated by a hemagglutinin (HA) tag as spacer, and a fusion of CUb to the C terminus of FKBP. G76 of CUb was mutated to valine (V) to provide resistance against cleavage by DUBs. When $^{NUb\text{-}FRB}$E3(63) was examined for activity toward $^{FKBP\text{-}CUb}$PCNA *in vitro*, the addition of Rapa strongly enhanced polyubiquitylation of the substrate (Figure S1D). However, we observed considerable background activity in the absence of the dimerizer and also toward a ^{CUb}PCNA construct lacking the FKBP domain. This was consistent with a reported residual affinity of NUb and CUb for each other.[24] We therefore introduced a mutation (I13A) into the NUb module (henceforth called NUa), which is known to lower the affinity for CUb (Figure S1A, step 3).[24] This mutation abolished all background activity (Figure S1D) and was therefore used for the final arrangement (Figure 1B). Application of the resulting tags, now called NUbo (NUa-HA-FRB) and CUbo (FKBP-CUb), to all three linkages thus resulted in the following engineered E3s: E3(1)^{CUbo}, ^{NUbo}E3(48), and ^{NUbo}E3(63) (Figure 1C).

In vitro validation of the Ubiquiton system

We used the green fluorescent protein (GFP) as a generic substrate to verify activity and specificity of the Ubiquiton components *in vitro*. Purified ^{NUbo}GFP was efficiently polyubiquitylated by E3(1)^{CUbo} in the presence of Rapa and a cognate E2, human UBCH7 (Figure 1D). Blocking the N terminus of the NUbo unit on GFP via a His_7-tag abolished all modification, while addition of an N-terminal myc-tag to free ubiquitin largely restricted chain elongation to a single ubiquitin unit. These data are consistent with E3(1)^{CUbo} forming an M1-linked polyubiquitin chain on the N terminus of ^{NUbo}GFP as intended. As noted for the PCNA-specific PIP-E3s,[18] we also observed formation of unanchored polyubiquitin chains and some auto-ubiquitylation of E3(1)^{CUbo} in these *in vitro* reactions (Figure S1E). Likely as a consequence

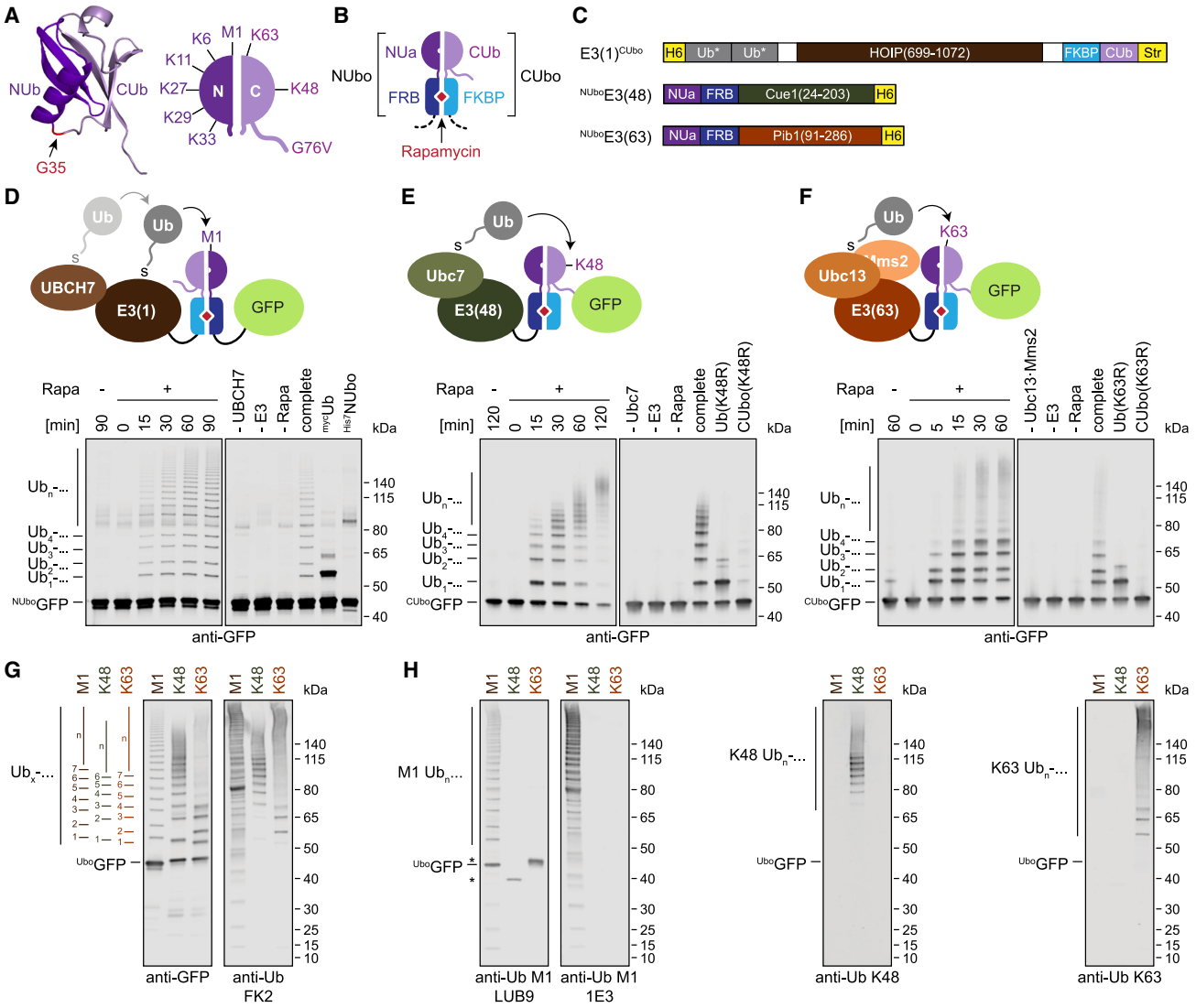

Figure 1. Design and *in vitro* validation of the Ubiquiton system

(A) Structure of ubiquitin (left, PDB: 1UBQ) and cartoon model of split ubiquitin (right), indicating separation point (G35) and distribution of lysines among the two halves, NUb and CUb.

(B) Design of the NUbo and CUbo modules. NUbo is an N-terminal fusion of NUb(I13A) to FRB(T2098L), separated by an HA-tag as spacer; CUbo is a C-terminal fusion of CUb(G76V) to FKBP.

(C) Domain arrangement of the Ubo-E3s. His_6- (H6) and/or TwinStrep- (Str) tags are for purification purposes. Numbers in brackets indicate the amino acids of the parent proteins. HOIP is human, Cue1 and Pib1 from budding yeast. Ub*: ubiquitin(K29R/K48R/K63R/G76L).

(D) Setup of the M1-Ubiquiton and *in vitro* activity toward a model substrate, $^{NUbo}GFP^{His6}$. Reactions with $^{His6}E3(1)^{CUbo\text{-}Str}$ and human $^{His6}UBCH7$ (E2) were incubated at 37°C under standard conditions with 5 μM rapamycin (Rapa) in the indicated time course or for 60 min with the indicated controls and analyzed by anti-GFP western blotting. Blots probed against ubiquitin and E3(1) are shown in Figure S1E.

(E) Setup of the K48-Ubiquiton and *in vitro* activity toward $^{His6\text{-}CUbo}GFP$. Reactions with $^{NUbo}E3(48)^{His6}$ and yeast $^{MBP}Ubc7^{His6}$ (E2) were incubated at 30°C under standard conditions with 5 μM rapamycin in the indicated time course, or for 30 min with the indicated controls, and analyzed by anti-GFP western blotting. Blots probed against ubiquitin and E3(48) are shown in Figure S1F.

(F) Setup of the K63-Ubiquiton and *in vitro* activity toward $^{His6\text{-}CUbo}GFP$. Reactions with $^{NUbo}E3(63)^{His6}$ and yeast $^{His6}Ubc13{\cdot}Mms2$ (E2) were incubated and analyzed as described in (E), but using a 15-min incubation for the control reactions. Blots probed against ubiquitin and E3(63) are shown in Figure S1G.

(G) Comparison of M1-, K48-, and K63-polyubiquitylation by Ubo-E3s. *In vitro* reactions as in (D)–(F) were incubated at 37°C for 90 min (M1), or at 30°C for 60 min (K48 and K63), and analyzed by western blotting against GFP and ubiquitin.

(H) Verification of linkages produced by the Ubo-E3s *in vitro*. Reactions as in (G) were probed with the indicated linkage-selective anti-ubiquitin antibodies. Note that the M1-specific antibody, LUB9, recognizes the N-terminal half of ubiquitin in the NUbo-module (*).

of producing E3(1)^{CUbo} in insect cells, ubiquitylated species of the E3 were also visible in the absence of E2 (Figure S1E).

K48-linked polyubiquitylation by ^{NUbo}E3(48) was tested with ^{CUbo}GFP (Figure 1E). Analogous to E3(1)^{CUbo}, modification depended on Rapa, the cognate E2 (here, budding yeast Ubc7), K48 of the substrate's CUbo module, and—for chain extension—K48 of the free ubiquitin used for conjugation. Levels of unanchored chain synthesis and auto-ubiquitylation of ^{NUbo}E3(48) were lower than with E3(1)^{CUbo} (Figure S1F). ^{NUbo}E3(63) yielded very similar results in reactions with its cognate E2, yeast Ubc13·Mms2, and ^{CUbo}GFP as a substrate (Figures 1F and S1G).

Side-by-side western blotting of the conjugates produced by the three Ubo-E3s revealed distinct migration patterns of the polyubiquitylated species, consistent with the different linkages (Figure 1G). Probing the blots with linkage-selective anti-ubiquitin antibodies verified the correct linkages for each E3 (Figure 1H). Taken together, these experiments confirm that the structural arrangement of the NUbo- and CUbo-tags allows for Rapa-induced re-assembly of the ubiquitin halves into a ubiquitin-like unit that can be recognized by the engineered E3s. Furthermore, they revealed the linkage-specific chain extension and high selectivity of all three E3s for the intended target site on ubiquitin.

The Ubiquiton tool affords linkage-selective polyubiquitylation in budding yeast and human cells

To test the efficacy of the Ubiquiton system in the environment of a cell, we initially chose the budding yeast, *S. cerevisiae*. Mutation of *TOR1* (S1972R, *TOR1-1*) and deletion of the gene encoding the endogenous Rapa-binding FKBP homolog, *FPR1*, rendered cells insensitive to Rapa, thus avoiding interference with induction conditions.[25] In addition, *PDR5*, encoding a plasma membrane multidrug transporter, was deleted to ensure effective use of proteasome inhibitors.[26]

We first established a "mono-Ubiquiton" by co-expressing a CUbo-tagged GFP with a non-catalytic fusion of NUbo to the vesicular stomatitis virus (VSV) tag to assess the effects of a permanently attached split-ubiquitin unit in yeast (Figure S2A). Upon Rapa treatment, ^{CUbo}GFP, but not ^{NUbo}VSV, was subject to low-level modification, likely indicating recognition by endogenous ligases. By introducing mutations in the two lysine residues present in the CUb unit, K48 and K63, we identified K48 as the main target of this endogenous response.

We then implemented the linkage-specific Ubiquiton arrangements with appropriately tagged GFP substrates. The final setup, shown in comparison with the mono-Ubiquiton as a time course (Figure 2A) and at steady state after overnight induction (Figure 2B), revealed distinctive polyubiquitylation patterns. Denaturing affinity purification of the substrates and blotting with linkage-selective anti-ubiquitin antibodies verified the intended linkages (Figure 2C). This final arrangement required several prior optimization steps and controls. For the M1-Ubiquiton, we codon-optimized the CUbo-tagged E3(1) for expression in yeast and tested a series of domain arrangements to prevent auto-modification and to maximize stability and activity *in vivo* (Figures S2B and S2C). In addition, we confirmed that blocking the N terminus of the substrate NUbo unit ($^{His7\text{-}NUbo}$GFP) or mutation of the catalytic cysteine of the E3 domain[27] (C885A of HOIP) abolished substrate modification (Figures S2D and S2E). Maximal activity of the K48- and K63-Ubiquiton was achieved by overexpression of the cognate E2s, whereas deletion of *UBC7* or *UBC13*, respectively, or mutating the designated acceptor lysine, reduced substrate ubiquitylation to background level (Figures S3A–S3D). A strong reduction in activity was also observed upon interfering with E2 recruitment—either by deleting the Ubc7-binding domain[28] of E3(48) (U7BD: aa 151–203 of Cue1) or by introducing a mutation into the catalytic RING finger[21] of E3(63) (I227A of Pib1) (Figures S3E and S3F). The background activity observed in a combination of ^{NUbo}E3(63) with a K63R mutant substrate was attributable to the same residual modification at K48 that we found to apply to the mono-Ubiquiton (Figures S3F and S3G). Finally, we found that the activity of all three Ubo-E3s was titratable by varying the Rapa concentration, reaching saturation around 2 μM (Figures S4A–S4C).

To further verify linkage selectivity in cells, we performed ubiquitin chain restriction (UbiCRest) analyses.[29] Three linkage-selective DUBs, OTULIN (M1), OTUB1 (K48), and AMSH (K63), were applied to affinity-purified GFP substrates from yeast extracts after treatment with Rapa. A promiscuous DUB, USP2cc,[30] served as control. Figures 2D–2F show that each set of conjugates was cleaved only by USP2cc and the cognate DUB. We also subjected affinity-purified GFP to stable isotope labeling by amino acids in cell culture- (SILAC) based or label-free mass spectrometry, using acceptor site mutants in the Ubo-tags and conditions without Rapa as controls (Figures S4D–S4F). In all cases, the expected linkage predominated among the detected diGlycine (diGly) peptides, thus confirming the linkage specificity of the E3s but providing no evidence for major branching *in vivo* (Figures S4G and S4H). The notion that no additional diGly peptides corresponding to the substrate were found confirms that all E3s are selective for chain extension versus *de novo* chain initiation.

The option of using the Ubiquiton in mammalian cells would greatly expand the potential of this tool. We therefore codon-optimized the Ubo-E3s for expression in human cells. As a model substrate, we chose histone H2B, which is normally subject to ubiquitylation at K120 in the context of transcriptional regulation, replication, and the DNA damage response.[31] For the M1-Ubiquiton, we co-expressed NUbo-tagged H2B with ^{myc}E3(1)^{CUbo}, analogous to the budding yeast construct. Rapa induced robust polyubiquitylation, detectable in whole-cell extracts by an antibody specific for linear polyubiquitin chains (Figures 3A). Mutation of the catalytic cysteine of ^{myc}E3(1)^{CUbo} (C885A) or blockage of the substrate acceptor site abolished polyubiquitylation of ^{NUbo}H2B. For the K48- and K63-Ubiquiton, we co-expressed His_8-tagged H2B^{CUbo} with ^{NUbo}E3(48) or ^{NUbo}E3(63), and codon-optimized versions of yeast Ubc7 or yeast Ubc13 and Mms2, respectively. Isolation of the substrate under denaturing conditions revealed polyubiquitylation upon Rapa addition and, as expected, K48R and K63R mutations in the CUbo-tag abolished modification with the corresponding linkage (Figures 3B and 3C).

In budding yeast, the tailor-made E3s exhibit little or no off-target activity.[18] To assess this in human cells, we performed SILAC-based diGly proteomics (Figure S5A) but found very few changes beyond a set of signals corresponding to the autoubiquitylation of the K63-specific enzymes themselves (Figures S5B–S5D).

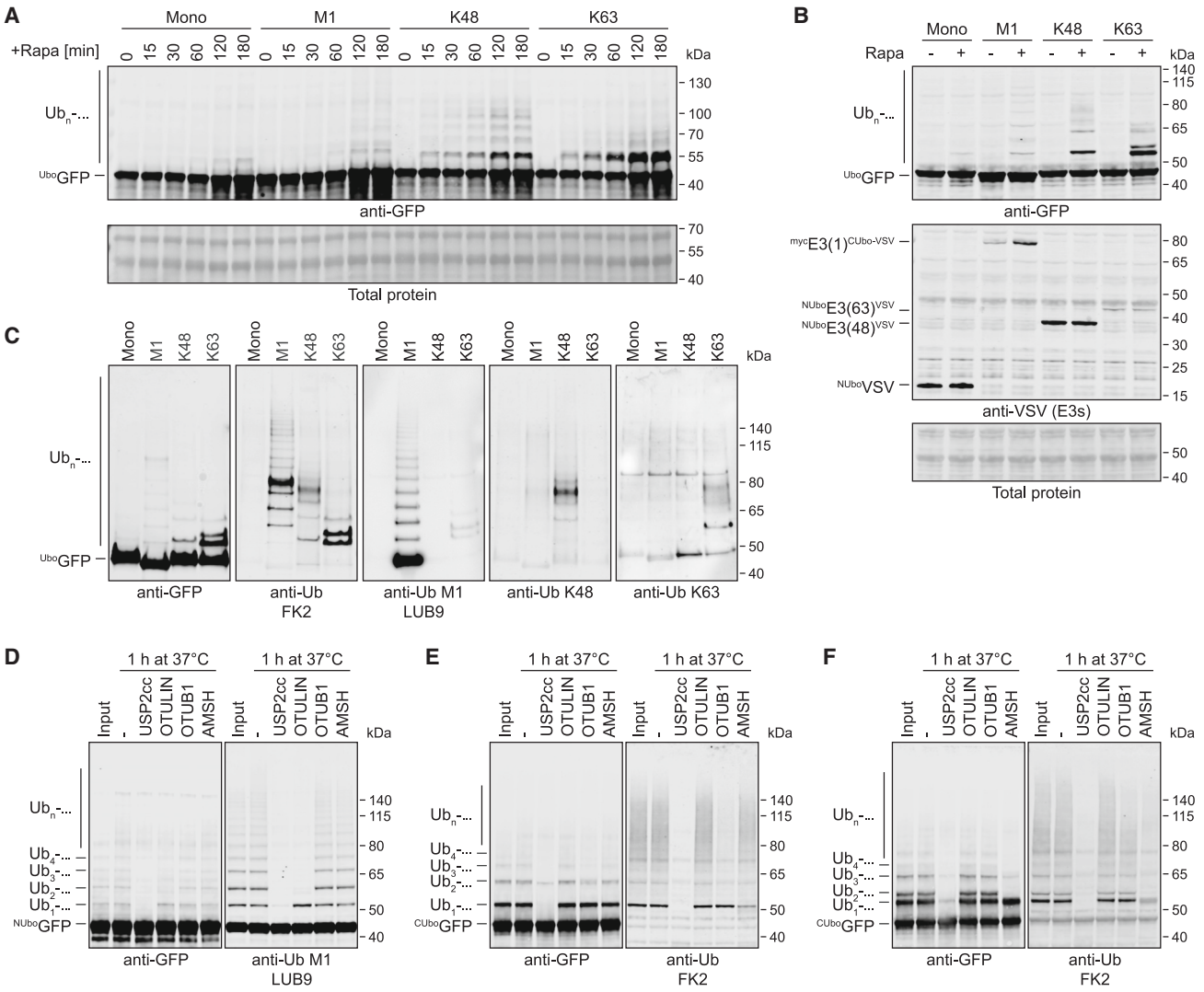

Figure 2. The Ubiquiton tool affords linkage-selective polyubiquitylation in yeast

(A) The optimized Ubiquiton setups induce polyubiquitylation of GFP model substrates in yeast. Diploid yeast cells expressing combinations of NUbo- and CUbo-tagged proteins were treated with rapamycin for the indicated times, and modification of GFP substrates was detected by western blotting of whole-cell lysates. Ponceau S staining (total protein) served as loading control. Mono: $^{His6\text{-}CUbo}$GFP and ^{NUbo}VSV; M1: ^{NUbo}GFP^{His6} and ^{myc}E3(1)$^{CUbo\text{-}VSV}$; K48: $^{His6\text{-}CUbo}$GFP and ^{NUbo}E3(48)^{VSV}, overexpression of *UBC7*; K63: $^{His6\text{-}CUbo}$GFP and ^{NUbo}E3(63)^{VSV}, overexpression of *UBC13* and *MMS2*. Optimization and controls for each linkage are shown in Figures S2 and S3.

(B) Steady-state levels of substrate ubiquitylation. Yeast strains described in (A) were incubated overnight in the absence or presence of rapamycin, and whole lysates were analyzed by western blotting against GFP (substrate), VSV (E3s), and Ponceau S staining.

(C) Verification of polyubiquitin chain linkage in yeast. Cells treated with rapamycin as in (B) were subjected to denaturing affinity purification of His_6-tagged GFP substrates. Samples were blotted and probed with anti-GFP, anti-ubiquitin, and linkage-selective anti-ubiquitin antibodies as indicated.

(D–F) UbiCRest analysis confirms the linkage of the polyubiquitin chains assembled *in vivo* by Ubo-E3s on their substrates. (D) M1-, (E) K48-, (F) K63-Ubiquiton. Yeast strains described in (A) were treated with rapamycin for 3 h. Substrates were affinity-purified under partially denaturing conditions and treated with the indicated DUBs. Bound material was analyzed by western blotting against GFP and ubiquitin.

Taken together, these experiments demonstrate a successful transfer of all three Ubo-E3s to yeast and human cells, with characteristics comparable to their *in vitro* behavior.

The K48-Ubiquiton acts as a degron

A K48-linked polyubiquitin chain is known to induce proteasomal degradation of the modified protein.[32] Hence, the K48-Ubiquiton should act as a degron. To assess this, we performed cycloheximide (CHX) chase experiments with ^{CUbo}GFP upon induction of the K48-Ubiquiton in *S. cerevisiae*. As expected, ^{CUbo}GFP was degraded upon Rapa treatment in a manner dependent on K48 of the substrate CUbo module and the Ubc7-binding domain of ^{NUbo}E3(48) (Figures 4A and S6A). Inhibition by MG132 demonstrated involvement of the proteasome

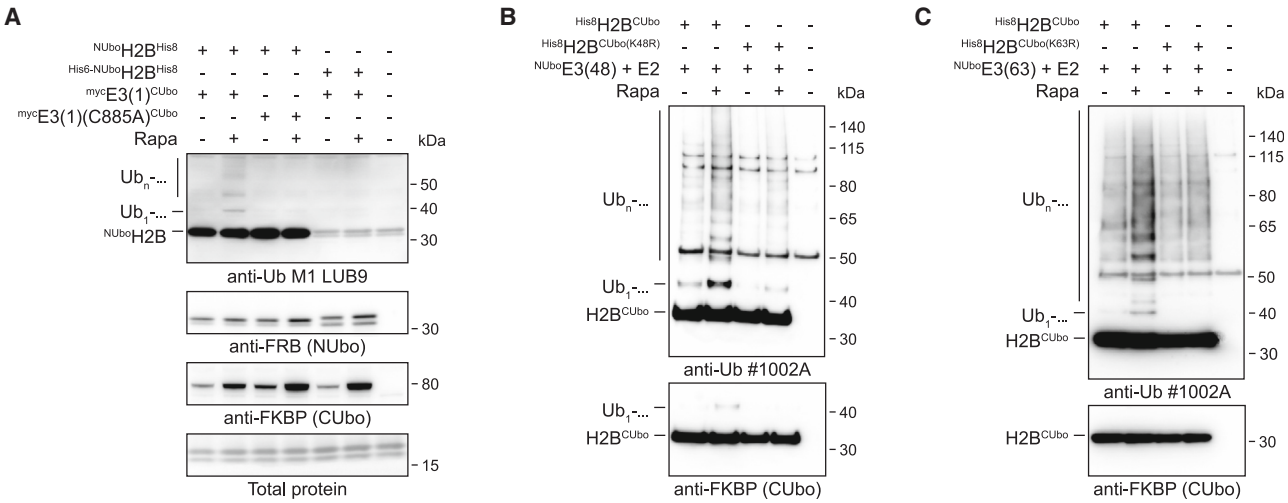

Figure 3. The Ubiquiton tool is applicable to human cells

(A) Polyubiquitylation of human H2B by the M1-Ubiquiton. HEK293T cells transfected with the indicated constructs were treated with DMSO or 1 μM rapamycin in DMSO for 4 h, and lysates were analyzed by western blotting against ubiquitin (LUB9), FRB (substrate), and FKBP (E3). Ponceau S staining served as loading control.

(B) Polyubiquitylation of human H2B by the K48-Ubiquiton. Cells transfected with the indicated constructs were treated as in (A), but for 30 min, and modifications were analyzed after nickel-nitriloacetic acid (Ni-NTA) pull-down of $^{His8}H2B^{CUbo}$ by western blotting using antibodies against ubiquitin and FKBP (substrate).

(C) Polyubiquitylation of human H2B by the K63-Ubiquiton. Cells transfected with the indicated constructs were treated and analyzed as in (B).

(Figure S6B), and degradation efficiency was titratable via the Rapa concentration (Figure S6C).

To benchmark the efficiency of the K48-Ubiquiton against an established degron, we inserted an auxin-inducible degron (AID*)[33,34] into our model substrate ($^{CUbo\text{-}AID*}$GFP) and introduced a cognate F-box protein, AFB2, into the host strain. The doubly tagged substrate was degradable by Rapa or auxin treatment, with comparable efficiency at saturating inducer levels (Figures 4B and S6D). Surprisingly, substrate ubiquitylation was detectable only after Rapa and not after auxin treatment (Figure S6D). A possible explanation might be a presumably more complex conjugate structure induced by the auxin-dependent ubiquitin conjugation system as compared with the single homotypic K48-chain generated by ^{NUbo}E3(48).

Because GFP is a notoriously problematic proteasome substrate[35,36] and was degraded inefficiently in our assays, we also tested the K48-Ubiquiton on essential endogenous yeast proteins. We chose two nuclear proteins, the DNA replication initiation factor Cdc45 and the DASH complex subunit Ask1, as well as the cytoplasmic septin Cdc11. For degradation of Cdc45 and Ask1, a nuclear localization signal (NLS) was fused to the C terminus of ^{NUbo}E3(48). Substrates were tagged alternatively with GFP alone, CUbo-GFP, AID*-GFP, or CUbo-AID*-GFP, and protein stability was monitored in parallel by colony formation upon chronic treatment on solid medium as well as short-term CHX chase and western blotting.

Under unchallenged conditions, the AID*-tag impaired growth when fused to Cdc11, while the CUbo-tag had no effect (Figure 4C). In fact, the AID*-tag partially destabilized all three substrates, explaining its adverse effect on Cdc11 (Figure S6E). When fused to Cdc45 or Ask1, the CUbo-tag was more effective and caused a stronger growth inhibition than the AID* degron (Figures 4C and 4D). On Cdc11, the AID*-tag proved ineffective, whereas the CUbo-tag afforded a significant reduction in protein levels under short-term treatment conditions, even though it impaired growth only in combination with the auxin-independent destabilizing effect of the AID*-tag (Figures 4C and 4D).

In summary, our data validate the K48-Ubiquiton as an inducible degron with comparable efficiency but orthogonal to the AID technology. In contrast to the AID*-tag, the CUbo-tag has no destabilizing effect in the absence of the inducer, which might prove advantageous in situations where native protein levels are required under unchallenged conditions.

Ubiquiton-mediated control over the fate of a yeast plasma membrane transporter

As a test case for proteasome-independent ubiquitin signaling, we chose the endocytic pathway, where mono- or K63-polyubiquitylation—in yeast largely mediated by the E3 Rsp5—induce internalization and lysosomal degradation of various plasma membrane proteins.[7] Localization and stability of the low-affinity hexose transporter, Hxt3, are normally regulated by the nature of the carbon source.[37] The involvement of Rsp5 suggests that Hxt3 undergoes mono- or K63-polyubiquitylation[38]; in a proteomics screen, the protein was in fact identified as K63-modified.[39] To dissect the consequences of Hxt3 ubiquitylation independently of nutrient availability and assess the relevance of linkage, we subjected the protein to Ubo-GFP-tagging in combination with Ubo-E3s and monitored localization and abundance by live-cell fluorescence microscopy and western blotting.

As expected,[38] Rapa induced internalization of $Hxt3^{GFP}$ and accumulation of the fluorescent signal in the vacuole of wild-type yeast. In contrast, the *TOR1-1 fpr1* background rendered $Hxt3^{GFP}$ insensitive to Rapa (Figure S7A). Assembly of a single

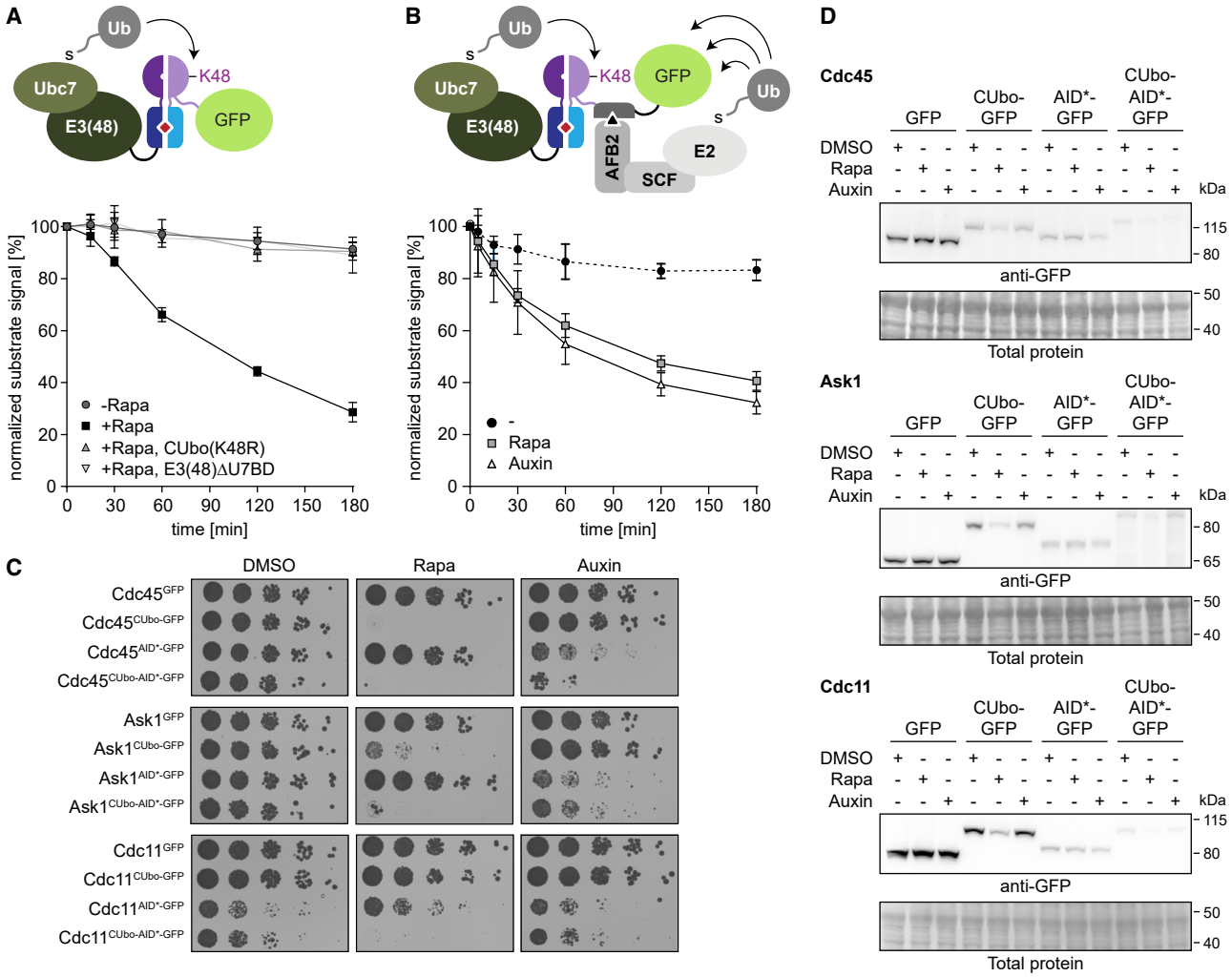

Figure 4. The K48-Ubiquiton acts as a degron

(A) The K48-Ubiquiton induces degradation of a model GFP substrate. Top: schematics of the K48-Ubiquiton. Bottom: diploid yeast cells expressing ^{NUbo}E3(48)^{VSV} and $^{His6\text{-}CUbo}$GFP or the indicated variants in a *pTDH3-UBC7* background were subjected to CHX chase in the presence or absence of rapamycin and relative substrate levels were quantified by western blotting (Figure S6A). The plot shows mean values and standard deviations of three independent experiments.

(B) The K48-Ubiquiton affords degradation at a rate comparable to the AID system. Top: schematics of the combined Ubo-AID* setup (triangle: auxin). Bottom: CHX chase assays as in (A), but with $^{CUbo\text{-}AID*}$GFP in strains harboring AFB2 (F-box protein) and using either rapamycin or auxin as inducer. The plot shows mean values and standard deviations of three independent experiments. Representative blots are shown in Figure S6D.

(C) Effects of AID*- and Ubo-mediated degradation of essential proteins on cell growth. Yeast strains expressing ^{NUbo}E3(48)^{VSV}, AFB2 (F-box protein), and *pTDH3-UBC7*, and harboring tagged alleles of *CDC11*, *ASK1*, or *CDC45* as indicated, were spotted in serial dilutions onto rich medium containing DMSO or 2 μM rapamycin in DMSO or 500 μM auxin. Plates were imaged after incubation for 2 days.

(D) Effects of AID*- and Ubo-mediated degradation on protein levels. Exponential cultures of the strains described in (C) were subjected to CHX chase in the presence of either DMSO or 2 μM rapamycin in DMSO or 500 μM auxin for 90 min. Protein levels were monitored by western blotting of whole-cell lysates against GFP. Ponceau S staining served as loading control.

ubiquitin on Hxt3 by the mono-Ubiquiton was insufficient to trigger endocytosis, as both Hxt3$^{CUbo\text{-}GFP}$ and ^{NUbo}Hxt3^{GFP} remained stably localized at the plasma membrane upon Rapa-induced dimerization with ^{NUbo}mCherry and ^{CUbo}mCherry, respectively (Figures 5A and 5B). Likewise, Rapa-induced recruitment of a full ubiquitin ($^{Ub*V\text{-}FRB}$mCherry) to Hxt3$^{FKBP\text{-}GFP}$ or permanent fusion of Hxt3 to a single non-extendable ubiquitin moiety (Hxt3$^{Ub*V\text{-}GFP}$) did not afford internalization or destabilization of the transporter (Figures S7B and S7C), indicating that a lack of proper folding of the split-ubiquitin unit was not responsible for the inactivity of the mono-Ubiquiton in inducing endocytosis. These findings contrast with other membrane proteins whose monoubiquitylation was reported to trigger internalization.[40,41] In the presence of ^{NUbo}E3(63)^{mCherry} and *UBC13·MMS2* overexpression, however, we observed efficient Rapa-induced endocytosis of Hxt3$^{CUbo\text{-}GFP}$, accompanied by a transient appearance of the fluorescent signal in internal vesicles, followed by an accumulation in the vacuole and the appearance

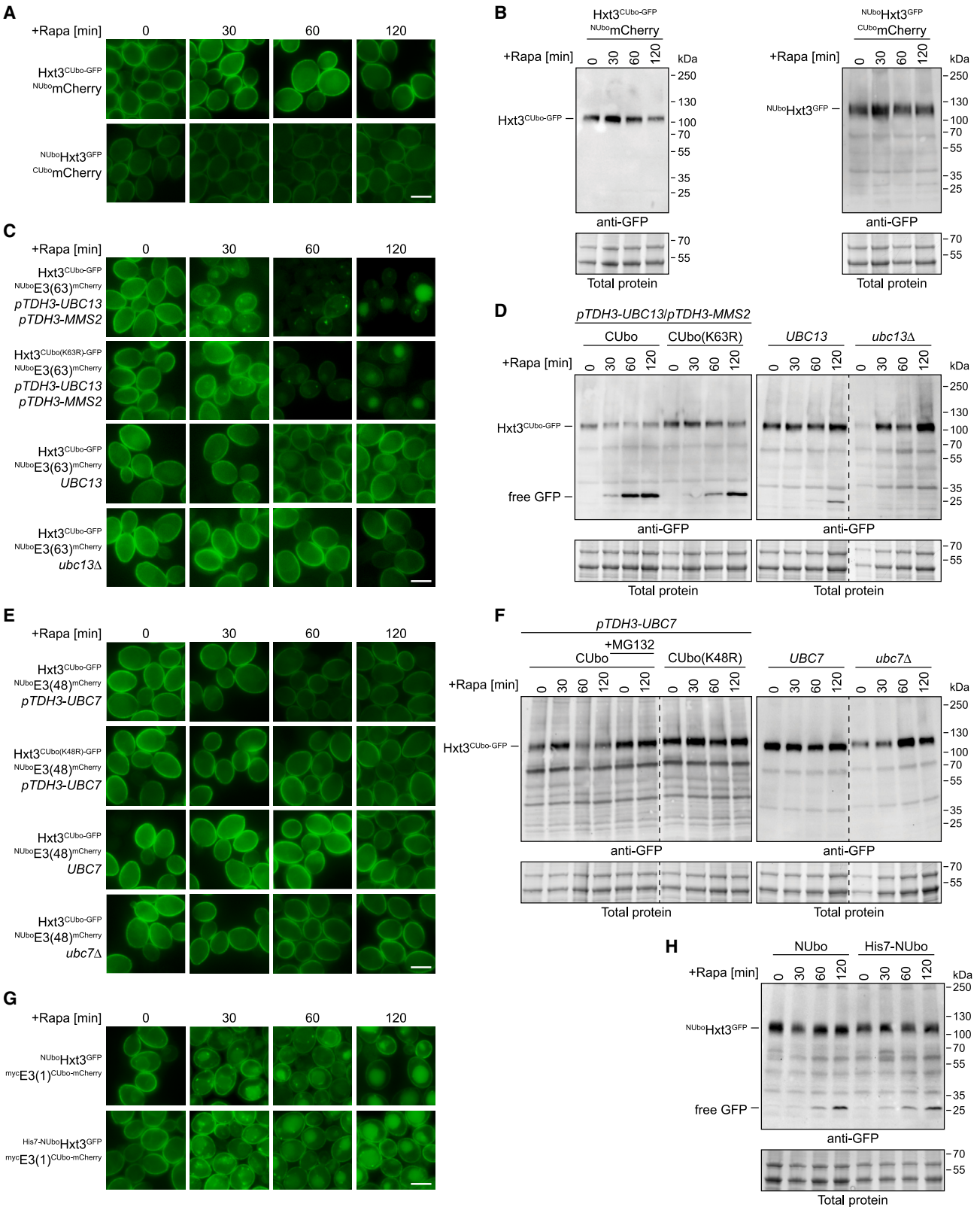

(legend on next page)

of free GFP on western blots, an indicator of vacuolar delivery (Figures 5C and 5D).

Endogenous levels of Ubc13 and Mms2 were less effective, and deletion of *UBC13* completely stabilized the transporter at the plasma membrane. This indicates that Ubc13·Mms2-mediated K63-polyubiquitylation serves as a trigger for endocytosis, independently of the physiological signal. Notably, mutation of K63 on the CUbo-tag of the substrate delayed but did not completely abolish Hxt3 endocytosis and vacuolar delivery, suggesting some chain-extending activity of the ^{NUbo}E3(63) toward other sites, either within Hxt3 (possibly via extension of monoubiquitin units attached by an endogenous E3) or on a neighboring protein whose polyubiquitylation would trigger bulk internalization of proteins in its vicinity. To differentiate between these scenarios, we isolated Hxt3$^{CUbo\text{-}GFP}$ under partially denaturing conditions and probed for ubiquitin. Figure S7D indicates robust polyubiquitylation of Hxt3$^{CUbo\text{-}GFP}$ but reduced levels in the K63R mutant. Thus, the efficiency of internalization and degradation of the substrate correlates with the degree of its ubiquitylation.

Unlike endogenous E3s, the Ubo-E3s offer the opportunity to examine the consequences of linkages not normally found on a given substrate. To explore a topologically distinct linkage, we therefore employed the K48-Ubiquiton. In cells expressing ^{NUbo}E3(48)^{mCherry} and overexpressing *UBC7*, we observed a Rapa-induced destabilization of Hxt3$^{CUbo\text{-}GFP}$, but without accumulation of the fluorescent signal in the vacuole (Figures 5E and 5F). Moreover, the absence of free GFP on western blots indicated that Hxt3$^{CUbo\text{-}GFP}$ is not degraded by the endocytic pathway. Instead, we found degradation to be dependent on proteasomal activity. Ubiquitylation (Figure S7E) and degradation were also abolished by a K48R mutation in the substrate's CUbo-tag. Reducing Ubc7 to wild-type levels or deleting *UBC7* likewise interfered with degradation (Figures 5E and 5F).

As a non-physiological linkage that is structurally similar to the K63-linkage but absent in yeast, we also probed the effect of linear polyubiquitylation by tagging Hxt3^{GFP} with an N-terminal NUbo-tag and expressing ^{myc}E3(1)$^{CUbo\text{-}mCherry}$ (Figures 5G and 5H). As with the K63-Ubiquiton, Rapa induced internalization and vacuolar degradation of the transporter. Surprisingly, blocking the acceptor site on the NUbo-tag (via an N-terminal His_7-tag) strongly reduced Hxt3 ubiquitylation (Figure S7F) but had no effect on internalization or vacuolar delivery. Endocytosis depended on the active-site cysteine of ^{myc}E3(1)$^{CUbo\text{-}mCherry}$ (Figures S7G and S7H). Thus, internalization of the blocked substrate likely indicates an activity of the E3 toward other proteins in the vicinity that triggers endocytosis of Hxt3.

Overall, these results demonstrate that polyubiquitin chain linkage determines the fate of a plasma-membrane-associated protein, with K63- or linear polyubiquitylation directing the substrate to the endocytic pathway, while K48-polyubiquitylation induces proteasomal degradation, possibly by direct extraction from the plasma membrane without prior internalization.

Ubiquiton-mediated control over EGFR localization and stability in human cells

As in budding yeast, endocytosis in human cells is governed by ubiquitylation.[42] The epidermal growth factor receptor (EGFR), a receptor tyrosine kinase important for cell proliferation and differentiation, utilizes two distinct routes of internalization. Low-level EGF signaling induces a clathrin-dependent pathway involving recycling of EGFR back to the plasma membrane, whereas high concentrations of the ligand mediate clathrin-independent endocytosis and lysosomal degradation.[43,44] EGF concentration directly controls the degree and duration of EGFR ubiquitylation, which in turn is thought to determine the internalization pathway.[45] The receptor is known to be modified by mono- and polyubiquitylation, predominantly but not exclusively via K63[46]; yet, the significance of the conjugate structure and its impact on endocytosis remain poorly understood. To address this in a defined setting independently of hormone signaling, we employed a truncated receptor, EGFR*, encompassing only the extracellular and transmembrane domains responsible for plasma membrane localization and unresponsive to EGF. When fused to a single ubiquitin moiety, this construct had previously been reported to undergo constitutive endocytosis and lysosomal degradation.[47] We now fused EGFR* to a CUbo-GFP tag for K48- or K63-modification (Figure S8A). As the N terminus of the receptor is oriented toward the external side of the plasma membrane, its topology is incompatible with the M1-Ubiquiton.

EGFR*$^{CUbo\text{-}GFP}$ was combined with ^{NUbo}E3s or—as a monoubiquitin mimic—a non-catalytic ^{NUbo}FLAG construct in HeLa cells deleted for endogenous EGFR. For the K48-Ubiquiton, we fused yeast Ubc7 to the C terminus of ^{NUbo}E3(48) via an *in vivo*-cleavable viral P2A peptide[48] in order to supply E3 and E2 via the same construct (Figure S8A). Polyubiquitylation of EGFR*$^{CUbo\text{-}GFP}$ by ^{NUbo}E3(48) and ^{NUbo}E3(63) upon Rapa treatment was confirmed by immunoprecipitation of the receptor and blotting for ubiquitin (Figure 6A). As intended, K48R or K63R mutations in the CUbo-tag of EGFR* interfered with ubiquitylation by the respective E3s, demonstrating site- and linkage-selective action of both enzymes. We then performed CHX chase experiments to assess EGFR*$^{CUbo\text{-}GFP}$

Figure 5. Ubiquiton-mediated control over a yeast plasma membrane transporter

(A and B) Mono-Ubiquiton at the N or C terminus of Hxt3 does not induce internalization. Yeast strains (*TOR1-1 fpr1Δ*) expressing the indicated constructs were treated with rapamycin at 30°C for the indicated times. Samples were analyzed by fluorescence microscopy (A) and western blotting (B). Total protein staining was used as loading control. Scale bars, 5 μm. Images of control strains are shown in Figure S7A.

(C and D) The K63-Ubiquiton induces endocytosis and vacuolar degradation of Hxt3 in a Ubc13-dependent manner. The indicated yeast strains were analyzed as in (A) and (B). The dashed line indicates removal of irrelevant lanes. Scale bars, 5 μm. K63-ubiquitylation of Hxt3$^{CUbo\text{-}GFP}$ is shown in Figure S7D.

(E and F) The K48-Ubiquiton targets Hxt3 for proteasomal degradation in a Ubc7-dependent manner. The indicated yeast strains were analyzed as in (A) and (B). Dashed lines indicate removal of irrelevant lanes. Scale bars, 5 μm. K48-ubiquitylation of Hxt3$^{CUbo\text{-}GFP}$ is shown in Figure S7E.

(G and H) The M1-Ubiquiton triggers endocytosis and vacuolar degradation of Hxt3. The indicated yeast strains were analyzed as in (A) and (B). Scale bars, 5 μm. Linear ubiquitylation of ^{NUbo}Hxt3^{GFP} is shown in Figure S7F.

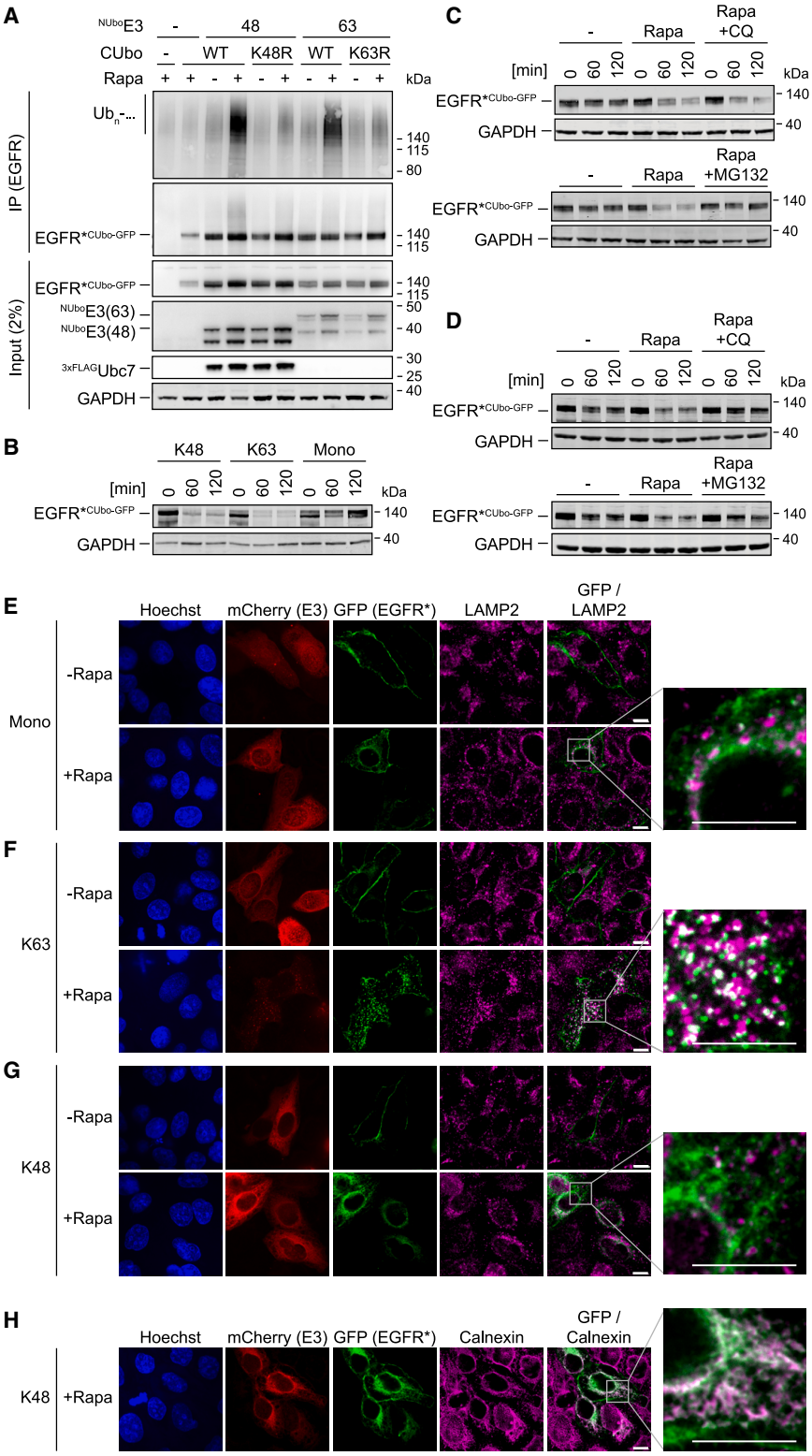

Figure 6. Ubiquiton-mediated control over EGFR localization and stability in human cells

(A) Ubiquiton-mediated polyubiquitylation of EGFR*. HeLa EGFR knockout cells expressing EGFR*$^{CUbo\text{-}GFP}$ and the indicated NUbo-E3 constructs (see Figure S8A) were treated with 1 μM rapamycin for 2 h, and polyubiquitylation of the receptor was analyzed by anti-EGFR immunoprecipitation and western blotting against ubiquitin (#1002A), GFP, FRB (E3s), and FLAG (Ubc7). Glyceraldehyde 3-phosphate dehydrogenase (GAPDH) served as loading control.

(B) Degradation of EGFR* is induced by K48- and K63-polyubiquitylation, but not by the mono-Ubiquiton. EGFR*$^{CUbo\text{-}GFP}$ levels were monitored in CHX chase assays. 24 h after co-transfection with EGFR*$^{CUbo\text{-}GFP}$ and NUbo constructs (^{NUbo}E3(48)$^{2A\text{-}3xFLAG}$Ubc7, ^{NUbo}E3(63)^{FLAG}, or ^{NUbo}FLAG), cells were pre-treated for 60 min with 50 μg·mL^{-1} CHX, and 1 μM rapamycin was added at t = 0. EGFR*$^{CUbo\text{-}GFP}$ was detected with an anti-GFP antibody; GAPDH served as loading control. Control blots are shown in Figure S8B.

(C) K48-linked polyubiquitylation of EGFR* induces proteasomal degradation. CHX chase assays were performed as in (B), but under conditions of lysosomal inhibition by 100 μM chloroquine (CQ) or proteasome inhibition by 30 μM MG132, where indicated. Detection was as in (B). Control blots are shown in Figure S8G.

(D) K63-linked polyubiquitylation induces lysosomal degradation. CHX chase assays were performed and analyzed as in (C). Control blots are shown in Figure S8H.

(E) The mono-Ubiquiton induces EGFR* internalization, but not lysosomal targeting. Confocal images of HeLa EGFR knockout cells transfected with EGFR*$^{CUbo\text{-}GFP}$ and ^{NUbo}mCherry^{FLAG} were acquired after 2 h treatment with DMSO or 1 μM rapamycin in DMSO. Nuclei were stained with Hoechst, and LAMP2, as a lysosomal marker, was detected with an Alexa Fluor 647-conjugated antibody. Scale bars, 10 μm.

(F) K63-polyubiquitylation induces EGFR* internalization and delivery to the lysosome. Confocal images were acquired as in (E) from cells expressing EGFR*$^{CUbo\text{-}GFP}$ and ^{NUbo}E3(63)$^{mCherry\text{-}FLAG}$. Scale bars, 10 μm.

(G) K48-polyubiquitylation induces accumulation of EGFR* around cell nuclei. Confocal images were acquired as in (E) from cells expressing EGFR*$^{CUbo\text{-}GFP}$ and ^{NUbo}E3(48)$^{mCherry\text{-}P2A\text{-}3xFLAG}$Ubc7. Scale bars, 10 μm.

(H) EGFR* co-localizes with the endoplasmic reticulum after K48-polyubiquitylation. Confocal images were acquired as in (E) from cells expressing EGFR*$^{CUbo\text{-}GFP}$ and ^{NUbo}E3(48)$^{mCherry\text{-}P2A\text{-}3xFLAG}$Ubc7. Calnexin was detected as a marker for the endoplasmic reticulum. Scale bars, 10 μm.

stability. Surprisingly, the mono-Ubiquiton—via dimerization with ^{NUbo}FLAG—had no effect. In contrast, both ^{NUbo}E3s afforded degradation (Figures 6B and S8B). K48-mediated degradation required the presence of yeast Ubc7 (Figure S8C) and ^{NUbo}E3(63) cooperated with the endogenous human Ubc13 homolog, UBE2N (Figure S8D). As expected, mutation of K48 or

K63 of the substrate's CUbo moiety impeded degradation (Figures S8E and S8F). To gain insight into the degradation pathways initiated by the respective ^{NUbo}E3s, we examined the susceptibility of EGFR*$^{CUbo\text{-}GFP}$ to the lysosomal inhibitor chloroquine (CQ) and the proteasome inhibitor MG132. K48-Ubiquiton-mediated degradation was prevented by MG132 but not by CQ, therefore implicating the proteasome in the process (Figures 6C and S8G). In contrast, CQ stabilized the receptor against ^{NUbo}E3(63)-mediated degradation, suggesting a lysosomal pathway (Figures 6D and S8H). MG132 also had a stabilizing effect, likely due to a depletion of the free ubiquitin pool.[49]

To examine how the various ubiquitin structures affected EGFR* trafficking, we followed the fate of EGFR*$^{CUbo\text{-}GFP}$ by confocal microscopy. Upon activation of the mono-Ubiquiton, we observed a partial redistribution of the chimeric receptor to intracellular vesicles (Figure 6E). However, these vesicles did not overlap with the lysosomal marker, LAMP2. This distribution, in combination with the observed lack of degradation (Figure 6B), is consistent with the clathrin-dependent internalization and subsequent recycling of EGFR induced by low-level EGF signaling.[43,44] In contrast and as expected, K63-polyubiquitylation afforded efficient internalization and co-localization of EGFR*$^{CUbo\text{-}GFP}$ with LAMP2, consistent with clathrin-independent lysosomal targeting (Figure 6F). Interestingly, upon K48-polyubiquitylation, EGFR*$^{CUbo\text{-}GFP}$ disappeared from the plasma membrane and accumulated at a network-like perinuclear structure distinct from the vesicles observed with mono- or K63-ubiquitylation (Figure 6G). Co-staining with calnexin identified this structure as the endoplasmic reticulum (Figure 6H).

In analogy to the yeast system, we finally confirmed the structural integrity of the mono-Ubiquiton by comparing its effect to that of a full non-extendable ubiquitin unit ($^{Ub*V\text{-}FRB}$mCherry) recruited to EGFR*$^{FKBP\text{-}GFP}$. Both arrangements induced some accumulation of the receptor in vesicles but without destabilizing the protein (Figures S8I and S8J), thus ruling out an artifact due to the split nature of the ubiquitin structure in the pair of Ubo-tags.

Taken together, these results reveal an activation of distinct internalization, intracellular redistribution, and/or degradation pathways by modification of EGFR* with defined ubiquitin conjugates, and they highlight the use of the Ubiquiton system as a promising tool for the analysis of ubiquitin-dependent protein trafficking.

DISCUSSION

Based on a set of engineered linkage-specific E3s, we have developed a modular toolbox for the induced modification of proteins with a monoubiquitin mimic as well as linear, K48-, or K63-polyubiquitin chains in yeast and human cells (Figure S9). We validated the system for soluble cytoplasmic and nuclear as well as membrane- and chromatin-associated proteins, demonstrating its broad applicability, and we show that its effects are tunable by varying the concentration of the inducer.

Our design relies on the ability of ubiquitin to re-assemble from two non-interacting peptides, each without biological activity in isolation. Although combination of split ubiquitin with the FKBP·FRB dimerization domains has been exploited in other techniques[50,51] for recognition by cellular DUBs with the purpose of controlling protein stability, we now demonstrate that split ubiquitin can also be harnessed in the form of stable fusions, either for extension by an E3 or as a monoubiquitin mimic.

The Ubiquiton system is complementary to a recently developed tool for site-specific, sortase-mediated monoubiquitylation via incorporation of a non-canonical amino acid at the designated modification site in the target protein.[52] However, although the approach permits the assembly of more complex conjugates *in vitro*,[53] polyubiquitylation has not been achieved in cells. Moreover, the need for genetic code expansion in the host cell introduces its own set of problems relating to variability of translation efficiency depending on the designated modification site.[54] Thus, the Ubiquiton system currently remains the only available tool for targeted linkage-selective polyubiquitylation in cells.

The K48-Ubiquiton as a degron

The K48-linkage was the first polyubiquitin chain topology to be identified as a proteasomal targeting signal.[32] Today, we know that ubiquitin conjugates promoting degradation are often more complex and may involve additional linkages such as K11 or K29.[4] Nevertheless, our results demonstrate that a presumably uniform chain initiating via K48 affords efficient degradation of a wide range of cellular proteins. This validates the K48-Ubiquiton as a degron orthogonal to other tools, such as the auxin-dependent AID system,[33] which facilitates experiments that require separate control over multiple different proteins in parallel. Although we have not tested our E3s in plant cells, the K48-Ubiquiton might circumvent problems associated with the use of auxin in plants. In yeast, the K48-Ubiquiton may often be preferable to PROTACs because of the inefficient uptake of such compounds in this organism.[55]

We found that even plasma-membrane-associated proteins that are normally internalized by the endocytic pathway can be re-routed to proteasomal degradation via K48-polyubiquitylation in yeast and human cells. AID technology and PROTACs have been applied to integral membrane proteins, but the structure of ubiquitin conjugates or the relevant degradation pathways have not been investigated.[56,57] The proteasome has been implicated in the physiological degradation of some plasma membrane receptors and K48-linkages have been detected on such proteins[58–60]; however, the relevance of this phenomenon has remained unclear, and interference with K63-mediated endocytosis has precluded systematic investigation of the underlying pathways. The K48-Ubiquiton should allow us to identify the factors involved and explore the extraction mechanism.

Insight into endocytosis from the Ubiquiton system

The impact of ubiquitylation on endocytosis is dauntingly complex, affecting both cargo proteins and the endocytic machinery itself.[7,42] The Ubiquiton system now permits a dissection of these processes independently of a biological signal by directing well-defined ubiquitin structures toward individual target proteins. The concept that K63-polyubiquitylation functions as a signal for the internalization of endocytic cargoes is based on the global impairment of endocytosis in yeast strains harboring a K63R mutation of ubiquitin[61–64] and the identification of K63-chains on numerous cargoes.[7] However, interference with

K63-polyubiquitylation may also alter other ubiquitin-dependent aspects of endocytosis, e.g., modification of the endocytic machinery itself.[65,66] Our data now reveal that K63-polyubiquitylation of a plasma membrane protein is sufficient to trigger its endocytosis in yeast and human cells.

In contrast, we found that a single ubiquitin unit was insufficient for lysosomal delivery. In yeast, it is conceivable that Hxt3 may require a higher degree of ubiquitylation than other plasma membrane proteins such as Ste2 or Pma1, where monoubiquitylation is sufficient for endocytosis.[40,41] In the human EGFR* system, a single ubiquitin unit promoted internalization but not lysosomal targeting. These findings support a previously proposed threshold model where each subsequent step in the internalization and trafficking of endocytic cargoes requires more extensive ubiquitylation.[45,46] They appear to contradict earlier results obtained with the EGFR*-ubiquitin chimera[47]; however, a possible explanation for this discrepancy is the long-term effect conveyed by permanent fusion of ubiquitin compared with our short-term induction. Moreover, K63-chain formation on the chimera over time was not excluded in the previous experiments. Thus, our use of the Ubiquiton system illustrates the importance of short-term inducible ubiquitylation for mechanistic studies.

Our finding that linear polyubiquitylation can substitute for the canonical K63-linkage in the internalization of a plasma membrane protein in yeast is reminiscent of an earlier report describing the sorting of a vacuolar membrane transporter into the vacuolar lumen by non-covalent association with a linear, non-cleavable tri-ubiquitin construct.[67] Similarly, linear chains can substitute for the physiological K63-polyubiquitylation of PCNA in the DNA damage tolerance pathway.[18] It will be interesting to explore whether this redundancy between two topologically similar chain types is limited to organisms without the capacity to assemble linear chains or whether it also applies to animals where both chain types co-exist and appear to fulfill distinct signaling functions.[68,69]

Limitations of the study

Several limitations still apply to the Ubiquiton system: at present, it depends on Rapa as an inducer, which complicates applications involving cellular target of rapamycin (TOR) signaling. Second, control over the length of the polyubiquitin chains assembled by the Ubo-E3s is presently possible only to some extent by adjusting the Rapa concentration. Moreover, we cannot exclude low-level modification by endogenous E3s, e.g., extension or branching with alternative linkages. Although the engineered E3s exhibit little or no off-target effects in yeast[18] or mammalian cells, modification of unintended targets, for example, those in the immediate vicinity of the cognate substrate, is possible. Mutation of the designated modification sites can control for this effect. Finally, the need for defined ubiquitin acceptor tags, dictated by the E3s' linkage specificities, necessitates an available N terminus for linear chain formation or the use of either the N or C terminus for K48- or K63-chains. Because modification is targeted toward these tags, induced polyubiquitylation at native modification sites is currently not possible. In cases where native attachment of ubiquitin is important, for example, to induce specific conformational changes, the Ubiquiton tool will therefore not be applicable. It should be noted, however, that polyubiquitin chains are generally recognized separately from their targets by dedicated binding domains,[3] which should allow for flexibility with respect to the modification site. Accordingly, there are numerous examples of the successful use of engineered linear N- or C-terminal ubiquitin fusion constructs in the literature,[23] whereas we are not aware of a single case where altering the position of a polyubiquitin chain was found to interfere with its functionality.

Outlook

For the future, we envision developments that will further expand the utility of the Ubiquiton tool. First and foremost, our study illustrates a general design principle that will allow the construction of conjugation factors selective for the rarer, non-canonical linkages, or even chain-branching enzymes, to expand the range of polyubiquitin chain geometries accessible to targeted assembly. Further, it will be important to explore the degree to which the Rapa-induced recruitment of Ubo-E3s is reversible. Alternative substrate-targeting modules would circumvent potential problems with the use of Rapa *in vivo*. Additional fusions of Ubo-E3s to their cognate E2s may enhance their efficiency and make the system more convenient for practical use.

Beyond its use as an efficient degron, we expect the Ubiquiton system to become a valuable resource for answering many outstanding questions pertaining to polyubiquitin chain linkage. Our Ubo-E3s could help differentiate between unique versus redundant roles of linear and K63-linked polyubiquitin chains, for example, in the context of inflammatory signaling.[68] They will facilitate dissecting the functional consequences of modification for the growing number of proteins found to be subject to both K48- and K63-polyubiquitylation, involving multiple or unknown E3s. Examples include the tumor suppressor p53,[70] RNA polymerase II,[71,72] various membrane receptors such as receptor tyrosine kinases,[58–60] kinase adaptors,[73] and autophagy substrates.[74] Inducing K48- and K63-modification separately by means of the Ubo-E3s will be key to understanding the underlying mechanisms of how the different conjugates are recognized and processed. Anchoring defined polyubiquitin structures to relevant subcellular locations, e.g., to organelles or at specified chromatin domains, should provide insight into ubiquitin signaling in pathways ranging from mitophagy to the DNA damage response. Finally, the ability to manipulate polyubiquitylation can contribute to controlling protein-protein interactions and signaling in synthetic biology applications. In this manner, our engineered writers complement the growing list of readers, erasers, and other reagents designed to investigate the ubiquitin code.

STAR★METHODS

Detailed methods are provided in the online version of this paper and include the following:

- KEY RESOURCES TABLE
- RESOURCE AVAILABILITY
  - Lead contact
  - Materials availability
  - Data and code availability

SUPPLEMENTAL INFORMATION

Supplemental information can be found online at https://doi.org/10.1016/j.molcel.2023.11.016.

ACKNOWLEDGMENTS

The authors thank Nils Johnsson, Robbie Loewith, Thomas U. Mayer, Simona Polo, Sara Sigismund, and Thomas Sommer for reagents. IMB's Core Facilities for Microscopy and Protein Production are acknowledged for their expert support and members of the Ulrich lab for critical comments and discussions. This project was funded by the Deutsche Forschungsgemeinschaft (DFG, German Research Foundation)—SFB 1551, project no. 464588647, and SFB 1361, project no. 393547839—a Research Training Network (UbiCODE, no. 765445) from the European Commission, and a Proof-of-Concept Grant (PoC 786330) from the European Research Council (ERC) to H.D.U. The Spinning Disk Confocal System (VisiScope 5-Elements, IMB, Microscopy Core Facility) was supported by the DFG (INST 247/912-1FUGG).

AUTHOR CONTRIBUTIONS

Conceptualization, C.R., S.W., and H.D.U.; investigation and formal analysis, C.R., E.A., C.M., V.A., K.P., N.C.K., S.W., A.F., and J.-X.C.; resources, H.-P.W. and R.P.W.; writing – original draft, C.R., E.A., and H.D.U.; writing – review & editing, all authors; supervision, S.L. and H.D.U.; funding acquisition, H.D.U.

DECLARATION OF INTERESTS

The authors declare no competing interests.

Received: April 7, 2023
Revised: September 28, 2023
Accepted: November 15, 2023
Published: December 15, 2023

REFERENCES

1. Komander, D., and Rape, M. (2012). The ubiquitin code. Annu. Rev. Biochem. *81*, 203–229.
2. Kwon, Y.T., and Ciechanover, A. (2017). The ubiquitin code in the ubiquitin-proteasome system and autophagy. Trends Biochem. Sci. *42*, 873–886.
3. Husnjak, K., and Dikic, I. (2012). Ubiquitin-binding proteins: decoders of ubiquitin-mediated cellular functions. Annu. Rev. Biochem. *81*, 291–322.
4. Kolla, S., Ye, M., Mark, K.G., and Rapé, M. (2022). Assembly and function of branched ubiquitin chains. Trends Biochem. Sci. *47*, 759–771.
5. Sasaki, K., and Iwai, K. (2023). Role of linear ubiquitination in inflammatory responses and tissue homeostasis. Int. Immunol. *35*, 19–25.
6. Wu, X., and Karin, M. (2015). Emerging roles of Lys63-linked polyubiquitylation in immune responses. Immunol. Rev. *266*, 161–174.
7. Erpapazoglou, Z., Walker, O., and Haguenauer-Tsapis, R. (2014). Versatile roles of k63-linked ubiquitin chains in trafficking. Cells *3*, 1027–1088.
8. Ulrich, H.D., and Walden, H. (2010). Ubiquitin signalling in DNA replication and repair. Nat. Rev. Mol. Cell Biol. *11*, 479–489.
9. Suryadinata, R., Roesley, S.N., Yang, G., and Sarčević, B. (2014). Mechanisms of generating polyubiquitin chains of different topology. Cells *3*, 674–689.
10. Sun, M., and Zhang, X. (2022). Current methodologies in protein ubiquitination characterization: from ubiquitinated protein to ubiquitin chain architecture. Cell Biosci. *12*, 126.
11. Leestemaker, Y., and Ovaa, H. (2017). Tools to investigate the ubiquitin proteasome system. Drug Discov. Today Technol. *26*, 25–31.
12. Spence, J., Sadis, S., Haas, A.L., and Finley, D. (1995). A ubiquitin mutant with specific defects in DNA repair and multiubiquitination. Mol. Cell. Biol. *15*, 1265–1273.
13. Xu, M., Skaug, B., Zeng, W., and Chen, Z.J. (2009). A ubiquitin replacement strategy in human cells reveals distinct mechanisms of IKK activation by TNFalpha and IL-1beta. Mol. Cell *36*, 302–314.
14. Dohmen, R.J., Wu, P., and Varshavsky, A. (1994). Heat-inducible degron: a method for constructing temperature-sensitive mutants. Science *263*, 1273–1276.
15. Prozzillo, Y., Fattorini, G., Santopietro, M.V., Suglia, L., Ruggiero, A., Ferreri, D., and Messina, G. (2020). Targeted protein degradation tools: overview and future perspectives. Biology (Basel) *9*, 421.
16. Békés, M., Langley, D.R., and Crews, C.M. (2022). Protac targeted protein degraders: the past is prologue. Nat. Rev. Drug Discov. *21*, 181–200.
17. Kozicka, Z., and Thomä, N.H. (2021). Haven't got a glue: protein surface variation for the design of molecular glue degraders. Cell Chem. Biol. *28*, 1032–1047.
18. Wegmann, S., Meister, C., Renz, C., Yakoub, G., Wollscheid, H.P., Takahashi, D.T., Mikicic, I., Beli, P., and Ulrich, H.D. (2022). Linkage reprogramming by tailor-made E3s reveals polyubiquitin chain requirements in DNA-damage bypass. Mol. Cell *82*, 1589–1602.e5.
19. Stieglitz, B., Rana, R.R., Koliopoulos, M.G., Morris-Davies, A.C., Schaeffer, V., Christodoulou, E., Howell, S., Brown, N.R., Dikic, I., and Rittinger, K. (2013). Structural basis for ligase-specific conjugation of linear ubiquitin chains by HOIP. Nature *503*, 422–426.
20. Bagola, K., von Delbrück, M., Dittmar, G., Scheffner, M., Ziv, I., Glickman, M.H., Ciechanover, A., and Sommer, T. (2013). Ubiquitin binding by a CUE domain regulates ubiquitin chain formation by ERAD E3 ligases. Mol. Cell *50*, 528–539.
21. Renz, C., Albanèse, V., Tröster, V., Albert, T.K., Santt, O., Jacobs, S.C., Khmelinskii, A., Léon, S., and Ulrich, H.D. (2020). Ubc13-Mms2 cooperates with a family of RING E3 proteins in budding yeast membrane protein sorting. J. Cell Sci. *133*, jcs244566.
22. Putyrski, M., and Schultz, C. (2012). Protein translocation as a tool: the current rapamycin story. FEBS Lett. *586*, 2097–2105.

23. Asimaki, E., Petriukov, K., Renz, C., Meister, C., and Ulrich, H.D. (2022). Fast friends - ubiquitin-like modifiers as engineered fusion partners. Semin. Cell Dev. Biol. *132*, 132–145.

24. Johnsson, N., and Varshavsky, A. (1994). Split ubiquitin as a sensor of protein interactions in vivo. Proc. Natl. Acad. Sci. USA. *91*, 10340–10344.

25. Heitman, J., Movva, N.R., and Hall, M.N. (1991). Targets for cell cycle arrest by the immunosuppressant rapamycin in yeast. Science *253*, 905–909.

26. Collins, G.A., Gomez, T.A., Deshaies, R.J., and Tansey, W.P. (2010). Combined chemical and genetic approach to inhibit proteolysis by the proteasome. Yeast *27*, 965–974.

27. Stieglitz, B., Morris-Davies, A.C., Koliopoulos, M.G., Christodoulou, E., and Rittinger, K. (2012). LUBAC synthesizes linear ubiquitin chains via a thioester intermediate. EMBO Rep. *13*, 840–846.

28. Kostova, Z., Mariano, J., Scholz, S., Koenig, C., and Weissman, A.M. (2009). A Ubc7p-binding domain in Cue1p activates ER-associated protein degradation. J. Cell Sci. *122*, 1374–1381.

29. Hospenthal, M.K., Mevissen, T.E.T., and Komander, D. (2015). Deubiquitinase-based analysis of ubiquitin chain architecture using ubiquitin Chain Restriction (UbiCRest). Nat. Protoc. *10*, 349–361.

30. Shahnawaz, M., Thapa, A., and Park, I.S. (2007). Stable activity of a deubiquitylating enzyme (Usp2-cc) in the presence of high concentrations of urea and its application to purify aggregation-prone peptides. Biochem. Biophys. Res. Commun. *359*, 801–805.

31. Mattiroli, F., and Penengo, L. (2021). Histone ubiquitination: an integrative signaling platform in genome stability. Trends Genet. *37*, 566–581.

32. Chau, V., Tobias, J.W., Bachmair, A., Marriott, D., Ecker, D.J., Gonda, D.K., and Varshavsky, A. (1989). A multiubiquitin chain is confined to specific lysine in a targeted short-lived protein. Science *243*, 1576–1583.

33. Nishimura, K., Fukagawa, T., Takisawa, H., Kakimoto, T., and Kanemaki, M. (2009). An auxin-based degron system for the rapid depletion of proteins in nonplant cells. Nat. Methods *6*, 917–922.

34. Morawska, M., and Ulrich, H.D. (2013). An expanded tool kit for the auxin-inducible degron system in budding yeast. Yeast *30*, 341–351.

35. Khmelinskii, A., Meurer, M., Ho, C.T., Besenbeck, B., Füller, J., Lemberg, M.K., Bukau, B., Mogk, A., and Knop, M. (2016). Incomplete proteasomal degradation of green fluorescent proteins in the context of tandem fluorescent protein timers. Mol. Biol. Cell *27*, 360–370.

36. Bragança, C.E., and Kraut, D.A. (2020). Mode of targeting to the proteasome determines GFP fate. J. Biol. Chem. *295*, 15892–15901.

37. Snowdon, C., and van der Merwe, G. (2012). Regulation of Hxt3 and Hxt7 turnover converges on the Vid30 complex and requires inactivation of the Ras/cAMP/PKA pathway in *Saccharomyces cerevisiae*. PLoS One *7*, e50458.

38. Yoshida, A., Wei, D., Nomura, W., Izawa, S., and Inoue, Y. (2012). Reduction of glucose uptake through inhibition of hexose transporters and enhancement of their endocytosis by methylglyoxal in *Saccharomyces cerevisiae*. J. Biol. Chem. *287*, 701–711.

39. Back, S., Gorman, A.W., Vogel, C., and Silva, G.M. (2019). Site-specific K63 Ubiquitinomics provides insights into translation regulation under stress. J. Proteome Res. *18*, 309–318.

40. Shih, S.C., Sloper-Mould, K.E., and Hicke, L. (2000). Monoubiquitin carries a novel internalization signal that is appended to activated receptors. EMBO J. *19*, 187–198.

41. Terrell, J., Shih, S., Dunn, R., and Hicke, L. (1998). A function for monoubiquitination in the internalization of a G protein-coupled receptor. Mol. Cell *1*, 193–202.

42. Acconcia, F., Sigismund, S., and Polo, S. (2009). Ubiquitin in trafficking: the network at work. Exp. Cell Res. *315*, 1610–1618.

43. Sigismund, S., Argenzio, E., Tosoni, D., Cavallaro, E., Polo, S., and Di Fiore, P.P. (2008). Clathrin-mediated internalization is essential for sustained EGFR signaling but dispensable for degradation. Dev. Cell *15*, 209–219.

44. Sigismund, S., Woelk, T., Puri, C., Maspero, E., Tacchetti, C., Transidico, P., Di Fiore, P.P., and Polo, S. (2005). Clathrin-independent endocytosis of ubiquitinated cargos. Proc. Natl. Acad. Sci. USA *102*, 2760–2765.

45. Akimov, V., Fehling-Kaschek, M., Barrio-Hernandez, I., Puglia, M., Bunkenborg, J., Nielsen, M.M., Timmer, J., Dengjel, J., and Blagoev, B. (2021). Magnitude of ubiquitination determines the fate of epidermal growth factor receptor upon ligand stimulation. J. Mol. Biol. *433*, 167240.

46. Huang, F., Kirkpatrick, D., Jiang, X., Gygi, S., and Sorkin, A. (2006). Differential regulation of EGF receptor internalization and degradation by multiubiquitination within the kinase domain. Mol. Cell *21*, 737–748.

47. Haglund, K., Sigismund, S., Polo, S., Szymkiewicz, I., Di Fiore, P.P., and Dikic, I. (2003). Multiple monoubiquitination of RTKs is sufficient for their endocytosis and degradation. Nat. Cell Biol. *5*, 461–466.

48. de Lima, J.G.S., and Lanza, D.C.F. (2021). 2A and 2A-like sequences: distribution in different virus species and applications in biotechnology. Viruses *13*, 2160.

49. Melikova, M.S., Kondratov, K.A., and Kornilova, E.S. (2006). Two different stages of epidermal growth factor (EGF) receptor endocytosis are sensitive to free ubiquitin depletion produced by proteasome inhibitor MG132. Cell Biol. Int. *30*, 31–43.

50. Pratt, M.R., Schwartz, E.C., and Muir, T.W. (2007). Small-molecule-mediated rescue of protein function by an inducible proteolytic shunt. Proc. Natl. Acad. Sci. USA *104*, 11209–11214.

51. Lau, H.D., Yaegashi, J., Zaro, B.W., and Pratt, M.R. (2010). Precise control of protein concentration in living cells. Angew. Chem. Int. Ed. Engl. *49*, 8458–8461.

52. Fottner, M., Brunner, A.D., Bittl, V., Horn-Ghetko, D., Jussupow, A., Kaila, V.R.I., Bremm, A., and Lang, K. (2019). Site-specific ubiquitylation and SUMOylation using genetic-code expansion and sortase. Nat. Chem. Biol. *15*, 276–284.

53. Fottner, M., Weyh, M., Gaussmann, S., Schwarz, D., Sattler, M., and Lang, K. (2021). A modular toolbox to generate complex polymeric ubiquitin architectures using orthogonal sortase enzymes. Nat. Commun. *12*, 6515.

54. Shandell, M.A., Tan, Z., and Cornish, V.W. (2021). Genetic code expansion: A brief history and perspective. Biochemistry *60*, 3455–3469.

55. Ernst, R., Klemm, R., Schmitt, L., and Kuchler, K. (2005). Yeast ATP-binding cassette transporters: cellular cleaning pumps. Methods Enzymol. *400*, 460–484.

56. Snyder, N.A., Kim, A., Kester, L., Gale, A.N., Studer, C., Hoepfner, D., Roggo, S., Helliwell, S.B., and Cunningham, K.W. (2019). Auxin-inducible depletion of the Essentialome suggests inhibition of TORC1 by auxins and inhibition of Vrg4 by SDZ 90–215, a natural antifungal cyclopeptide. G3 (Bethesda) *9*, 829–840.

57. Ruffilli, C., Roth, S., Rodrigo, M., Boyd, H., Zelcer, N., and Moreau, K. (2022). Proteolysis targeting chimeras (PROTACs): A perspective on integral membrane protein degradation. ACS Pharmacol. Transl. Sci. *5*, 849–858.

58. Marx, C., Held, J.M., Gibson, B.W., and Benz, C.C. (2010). ErbB2 trafficking and degradation associated with K48 and K63 polyubiquitination. Cancer Res. *70*, 3709–3717.

59. Meijer, I.M., van Rotterdam, W., van Zoelen, E.J., and van Leeuwen, J.E. (2013). Cbl and Itch binding sites in ERBB4 CYT-1 and CYT-2 mediate K48- and K63-polyubiquitination, respectively. Cell. Signal. *25*, 470–478.

60. Huang, F., Zeng, X., Kim, W., Balasubramani, M., Fortian, A., Gygi, S.P., Yates, N.A., and Sorkin, A. (2013). Lysine 63-linked polyubiquitination is required for EGF receptor degradation. Proc. Natl. Acad. Sci. USA *110*, 15722–15727.

61. Galan, J.M., and Haguenauer-Tsapis, R. (1997). Ubiquitin lys63 is involved in ubiquitination of a yeast plasma membrane protein. EMBO J. *16*, 5847–5854.

62. Erpapazoglou, Z., Froissard, M., Nondier, I., Lesuisse, E., Haguenauer-Tsapis, R., and Belgareh-Touzé, N. (2008). Substrate- and ubiquitin-dependent trafficking of the yeast siderophore transporter Sit1. Traffic *9*, 1372–1391.

63. Paiva, S., Vieira, N., Nondier, I., Haguenauer-Tsapis, R., Casal, M., and Urban-Grimal, D. (2009). Glucose-induced ubiquitylation and endocytosis of the yeast Jen1 transporter: role of lysine 63-linked ubiquitin chains. J. Biol. Chem. *284*, 19228–19236.

64. Kim, Y., Deng, Y., and Philpott, C.C. (2007). GGA2- and ubiquitin-dependent trafficking of Arn1, the ferrichrome transporter of *Saccharomyces cerevisiae*. Mol. Biol. Cell *18*, 1790–1802.

65. Stamenova, S.D., Dunn, R., Adler, A.S., and Hicke, L. (2004). The Rsp5 ubiquitin ligase binds to and ubiquitinates members of the yeast CIN85-endophilin complex, Sla1-Rvs167. J. Biol. Chem. *279*, 16017–16025.

66. Dores, M.R., Schnell, J.D., Maldonado-Baez, L., Wendland, B., and Hicke, L. (2010). The function of yeast epsin and Ede1 ubiquitin-binding domains during receptor internalization. Traffic *11*, 151–160.

67. Zhu, L., Jorgensen, J.R., Li, M., Chuang, Y.S., and Emr, S.D. (2017). ESCRTs function directly on the lysosome membrane to downregulate ubiquitinated lysosomal membrane proteins. eLife *6*, e26403.

68. Cohen, P., and Strickson, S. (2017). The role of hybrid ubiquitin chains in the MyD88 and other innate immune signalling pathways. Cell Death Differ. *24*, 1153–1159.

69. Iwai, K. (2021). LUBAC-mediated linear ubiquitination: a crucial regulator of immune signaling. Proc. Jpn. Acad. Ser. B Phys. Biol. Sci. *97*, 120–133.

70. Guo, Y., Li, Q., Zhao, G., Zhang, J., Yuan, H., Feng, T., Ou, D., Gu, R., Li, S., Li, K., et al. (2021). Loss of TRIM31 promotes breast cancer progression through regulating K48- and K63-linked ubiquitination of p53. Cell Death Dis. *12*, 945.

71. Harreman, M., Taschner, M., Sigurdsson, S., Anindya, R., Reid, J., Somesh, B., Kong, S.E., Banks, C.A., Conaway, R.C., Conaway, J.W., and Svejstrup, J.Q. (2009). Distinct ubiquitin ligases act sequentially for RNA polymerase II polyubiquitylation. Proc. Natl. Acad. Sci. USA *106*, 20705–20710.

72. Nakazawa, Y., Hara, Y., Oka, Y., Komine, O., van den Heuvel, D., Guo, C., Daigaku, Y., Isono, M., He, Y., Shimada, M., et al. (2020). Ubiquitination of DNA damage-stalled RNAPII promotes transcription-coupled repair. Cell *180*, 1228–1244.e24.

73. Newton, K., Matsumoto, M.L., Wertz, I.E., Kirkpatrick, D.S., Lill, J.R., Tan, J., Dugger, D., Gordon, N., Sidhu, S.S., Fellouse, F.A., et al. (2008). Ubiquitin chain editing revealed by polyubiquitin linkage-specific antibodies. Cell *134*, 668–678.

74. Wang, Y.T., Liu, T.Y., Shen, C.H., Lin, S.Y., Hung, C.C., Hsu, L.C., and Chen, G.C. (2022). K48/K63-linked polyubiquitination of ATG9A by TRAF6 E3 ligase regulates oxidative stress-induced autophagy. Cell Rep. *38*, 110354.

75. Stelter, P., and Ulrich, H.D. (2003). Control of spontaneous and damage-induced mutagenesis by SUMO and ubiquitin conjugation. Nature *425*, 188–191.

76. Neuber, O., Jarosch, E., Volkwein, C., Walter, J., and Sommer, T. (2005). Ubx2 links the Cdc48 complex to ER-associated protein degradation. Nat. Cell Biol. *7*, 993–998.

77. Ulrich, H.D. (2003). Protein-protein interactions within an E2-ring finger complex. Implications for ubiquitin-dependent DNA damage repair. J. Biol. Chem. *278*, 7051–7058.

78. Finley, D., Ozkaynak, E., and Varshavsky, A. (1987). The yeast polyubiquitin gene is essential for resistance to high temperatures, starvation, and other stresses. Cell *48*, 1035–1046.

79. Cox, J., and Mann, M. (2008). MaxQuant enables high peptide identification rates, individualized p.p.b.-range mass accuracies and proteome-wide protein quantification. Nat. Biotechnol. *26*, 1367–1372.

80. Phipson, B., Lee, S., Majewski, I.J., Alexander, W.S., and Smyth, G.K. (2016). Robust hyperparameter estimation protects against hypervariable genes and improves power to detect differential expression. Ann. Appl. Stat. *10*, 946–963.

81. Perez-Riverol, Y., Bai, J., Bandla, C., García-Seisdedos, D., Hewapathirana, S., Kamatchinathan, S., Kundu, D.J., Prakash, A., Frericks-Zipper, A., Eisenacher, M., et al. (2022). The PRIDE database resources in 2022: a hub for mass spectrometry-based proteomics evidences. Nucleic Acids Res. *50*, D543–D552.

82. Emmerich, C.H., and Cohen, P. (2015). Optimising methods for the preservation, capture and identification of ubiquitin chains and ubiquitylated proteins by immunoblotting. Biochem. Biophys. Res. Commun. *466*, 1–14.

83. Fujimuro, M., Sawada, H., and Yokosawa, H. (1994). Production and characterization of monoclonal antibodies specific to multi-ubiquitin chains of polyubiquitinated proteins. FEBS Lett. *349*, 173–180.

84. Janke, C., Magiera, M.M., Rathfelder, N., Taxis, C., Reber, S., Maekawa, H., Moreno-Borchart, A., Doenges, G., Schwob, E., Schiebel, E., and Knop, M. (2004). A versatile toolbox for PCR-based tagging of yeast genes: new fluorescent proteins, more markers and promoter substitution cassettes. Yeast *21*, 947–962.

85. Pickart, C.M., and Raasi, S. (2005). Controlled synthesis of polyubiquitin chains. Methods Enzymol. *399*, 21–36.

86. Carvalho, A.F., Pinto, M.P., Grou, C.P., Vitorino, R., Domingues, P., Yamao, F., Sá-Miranda, C., and Azevedo, J.E. (2012). High-yield expression in *Escherichia coli* and purification of mouse ubiquitin-activating enzyme E1. Mol. Biotechnol. *51*, 254–261.

87. Davies, A.A., and Ulrich, H.D. (2012). Detection of PCNA modifications in *Saccharomyces cerevisiae*. Methods Mol. Biol. *920*, 543–567.

88. Hughes, C.S., Moggridge, S., Müller, T., Sorensen, P.H., Morin, G.B., and Krijgsveld, J. (2019). Single-pot, solid-phase-enhanced sample preparation for proteomics experiments. Nat. Protoc. *14*, 68–85.

89. Rappsilber, J., Ishihama, Y., and Mann, M. (2003). Stop and go extraction tips for matrix-assisted laser desorption/ionization, nanoelectrospray, and LC/MS sample pretreatment in proteomics. Anal. Chem. *75*, 663–670.

90. Cox, J., Neuhauser, N., Michalski, A., Scheltema, R.A., Olsen, J.V., and Mann, M. (2011). Andromeda: a peptide search engine integrated into the MaxQuant environment. J. Proteome Res. *10*, 1794–1805.

CellPress
OPEN ACCESS

STAR★METHODS

KEY RESOURCES TABLE

REAGENT or RESOURCE	SOURCE	IDENTIFIER
Antibodies		
Rabbit polyclonal anti-PCNA (*S. cerevisiae*)	Stelter et al.[75]	N/A
Mouse monoclonal anti-GFP (clone 7.1/13.1)	Roche	Cat# 11814460001;RRID:AB_390913
Rabbit polyclonal anti-GFP	Thermo Fisher Scientific	Cat# A-6455; RRID:AB_221570
Mouse monoclonal anti-RFP (clone 6G6)	ChromoTek/Proteintech	Cat# 6g6; RRID:AB_2631395
Rabbit polyclonal anti-FKBP12	Enzo Life Sciences	Cat# ALX-210-142-R100;RRID:AB_2051415
Rabbit polyclonal mTOR (human FRB domain)	Enzo Life Sciences	Cat# ALX-215-065-1; RRID:AB_2051920
Mouse monoclonal anti-ubiquitin (clone FK2)	Merck KgaA	Cat# 04-263; RRID:AB_612093
Rabbit monoclonal anti-ubiquitin (clone #1002A)	R&D Systems	Cat# MAB8595RRID:AB_2928999
Mouse monoclonal anti-ubiquitin (clone P4D1)	Cell Signaling Technologies	Cat# 3936; RRID:AB_331292
Mouse monoclonal anti-ubiquitin (clone VU-1)	LifeSensors	Cat# VU101; RRID:AB_2716558
Rabbit monoclonal anti-ubiquitin-K48 (clone Apu2)	Merck KgaA	Cat# 05-1307; RRID:AB_1587578
Rabbit monoclonal anti-ubiquitin-K48 (clone Apu2)	Merck KgaA	Cat# ZRB2150; RRID:AB_2928997
Rabbit monoclonal anti-ubiquitin-K63 (clone Apu3)	Merck KgaA	Cat# 05-1308; RRID:AB_1587580
Rabbit monoclonal anti-ubiquitin-M1 (clone 1E3)	Merck KgaA	Cat# MABS199; RRID:AB_2576212
Mouse monoclonal anti-ubiquitin-M1 (clone LUB9)	Merck KgaA	Cat# MABS451; RRID:AB_2929000
Rabbit polyclonal anti-Ubc7 (*S. cerevisiae*)	Neuber et al.[76]	N/A
Rabbit polyclonal anti-Ubc13 (*S. cerevisiae*)	Ulrich[77]	N/A
Rabbit polyclonal anti-Mms2 (*S. cerevisiae*)	In-house	N/A
Rabbit monoclonal anti-α-tubulin (clone EPR13799)	Abcam	Cat# ab184970; RRID:AB_2928998
Mouse monoclonal anti-VSV (clone P5D4)	Merck KgaA	Cat# SAB4200695;RRID:AB_2929001
Mouse monoclonal anti-FLAG (clone M2)	Merck KgaA	Cat# F1804; RRID:AB_262044
Mouse monoclonal anti-EGFR (*H. sapiens*, clone H11)	Thermo Fisher Scientific	Cat# MA5-13070; RRID:AB_10977527
Mouse monoclonal anti-p53 (*H. sapiens*, clone do-1)	Santa Cruz Biotechnology	Cat# sc-126; RRID:AB_628082
Rabbit polyclonal anti-UBE2N (*H. sapiens*)	Cell Signaling Technology	Cat# 4919; RRID:AB_2211168
Goat polyclonal anti-GAPDH (*H. sapiens*)	Novus	Cat# NB300-320; RRID:AB_10001796
Mouse monoclonal anti-LAMP2 (*H. sapiens*, clone H4B4)	Santa Cruz Biotechnology	Cat# sc-18822; RRID:AB_626858
Rabbit polyclonal anti-Calnexin (*H. sapiens*)	Abcam	Cat# ab22595; RRID:AB_2069006
IRDye® 680LT donkey anti-rabbit IgG secondary antibody	LI-COR	Cat# 926-68023; RRID:AB_10706167

(*Continued on next page*)

Continued

REAGENT or RESOURCE	SOURCE	IDENTIFIER
IRDye® 680RD donkey anti-mouse IgG secondary antibody	LI-COR	Cat# 926-68072; RRID:AB_10953628
IRDye® 800CW goat anti-rabbit IgG secondary antibody	LI-COR	Cat# 926-32211; RRID:AB_621843
IRDye® 800CW donkey anti-mouse IgG secondary antibody	LI-COR	Cat# 926-32212; RRID:AB_621847
IRDye® 800CW donkey anti-goat IgG secondary antibody	LI-COR	Cat# 926-32214; RRID:AB_621846
Polyclonal goat anti-mouse IgG secondary antibody, HRP	Agilent	Cat# P0447; RRID:AB_2617137
Polyclonal goat anti-mouse IgG secondary antibody, HRP	Merck KgaA	Cat# A5278; RRID:AB_258232
Polyclonal goat anti-rabbit Ig secondary antibody, HRP	Agilent	Cat# P0448;RRID:AB_2617138
Polyclonal goat anti-rabbit IgG (H+L) secondary antibody, Alexa Fluor 647, cross-adsorbed	Thermo Fisher Scientific	Cat# A-21244; RRID:AB_2535812
Bacterial strains		
Escherichia coli Top10	Thermo Fisher Scientific	Cat# C404010
Escherichia coli BL21(DE3)	Merck KgaA	Cat# 69450
Escherichia coli BL21(DE3)pLysS	Merck KgaA	Cat# 69451
Escherichia coli BL21-CodonPlus(DE3)-RIL	Agilent Technologies	Cat# 230240
Escherichia coli Rosetta™ 2(DE3)pLysS	Merck KgaA	Cat# 71403
Chemicals, peptides, and recombinant proteins		
Ubiquitin from bovine erythrocytes	Merck KgaA	Cat# U6253
Pfu Turbo DNA Polymerase	Agilent	Cat# 600250
Serratia marcescens Nuclease (SmNuclease)	In-house	N/A
Thrombin Cleavage Capture Kit	Merck KgaA	Cat# 69022
Bovine serum albumin (BSA)	Merck KgaA	Cat# A7906
SIGMAFAST protease inhibitor cocktail	Merck KgaA	Cat# S8830
cOmplete™, Mini, EDTA-free	Roche	Cat# 5056489001
Phenylmethanesulfonyl fluoride (PMSF)	Merck KgaA	Cat# P7626
N-Ethylmaleimide (NEM)	Merck KgaA	Cat# E3876
Ni-NTA agarose	Qiagen	Cat# 30250
Glutathione Sepharose	Cytiva	Cat# 17-5132-02
Magnetic agarose GFP binder beads	In-house	N/A
Protein G agarose, >98%	Merck KgaA	Cat# 11243233001
Beads for BeadBeater® Zirconia/glass beads, 0.5 mm	Carl Roth	Cat# N034.1
Imidazole	Merck KgaA	Cat# I2399
Glutathione	Merck KgaA	Cat# G4251
Isopropyl β-D-1-thiogalactopyranoside (IPTG)	Generon	Cat# GEN-S-02122
Adenosine 5′-triphosphate (ATP)	New England Biolabs	Cat# P0756
DL-dithiothreitol (DTT)	Merck KgaA	Cat# D0632
D-desthiobiotin	IBA Lifesciences	Cat# 2-1000-001
Tris(2-carboxyethyl)phosphine hydrochloride solution (TCEP)	Merck KgaA	Cat# 646547
Dimethyl sulfoxide (DMSO)	Merck KgaA	Cat# D8418
Rapamycin	Biozol	Cat# SEL-S1039

(*Continued on next page*)

Continued

REAGENT or RESOURCE	SOURCE	IDENTIFIER
Rapamycin	Merck KgaA	Cat# 55321
Rapamycin	Thermo Fisher Scientific	Cat# PHZ1235
Rapamycin	LC Laboratories	Cat# R-5000
Auxin (indole-3-acetic acid sodium salt)	Cayman Chemicals	Cat# 16954
5-Fluoroorotic acid monohydrate (5-FOA)	Toronto Research Chemicals	Cat# F595000
Cycloheximide (CHX)	Merck KgaA	Cat# C7698
MG132	Enzo Life Sciences	Cat# BML-PI102-0025
Chloroquine (CQ)	Merck KgaA	Cat# C6628
Copper sulfate	Merck KgaA	Cat# C1297
Trichloroacetic acid (TCA)	Merck KgaA	Cat# T8657
Trichloroacetic acid (TCA) solution, 6.1 N	Merck KgaA	Cat# T0699
2-Mercaptoethanol	Merck KgaA	Cat# M3148
Triton X-100	Merck KgaA	Cat# T9284
Sodium deoxycholate	Merck KgaA	Cat# D6750
Sodium dodecyl sulfate (SDS), 20%	Merck KgaA	Cat# 05030
Tween-20	Merck KgaA	Cat# P7949
Urea	Merck KgaA	Cat# U6504
Guanidine hydrochloride	Carl Roth	Cat# 0037.1
L-lysine-0 [L-lysine monohydrochloride]	Merck KgaA	L8662
L-lysine-4 [L-lysine:2HCl (4,4,5,5-D_4)]	Cambridge Isotope Laboratories	DLM-2640-1
L-lysine-8 [L-lysine:2HCl ($^{13}C_6$, $^{15}N_2$)]	Cambridge Isotope Laboratories	CNLM-291-H-1
L-arginine-0 [L-arginine monohydrochloride]	Merck KgaA	A6969
L-arginine-10 [L-arginine:HCl ($^{13}C_6$, $^{15}N_4$)]	Cambridge Isotope Laboratories	CNLM-539-H-1
PTMScan® Ubiquitin Remnant Motif (K-ε-GG) Kit	Cell Signaling Technology	Cat# 5562
Dulbecco's Modified Eagle Medium (DMEM)	Thermo Fisher Scientific	Cat# 11995065
Sf-900™ III Serum-Free Medium	Thermo Fisher Scientific	Cat# 12658027
Penicillin-Streptomycin (10,000 U·mL^{-1})	Thermo Fisher Scientific	Cat# 15140122
Lipofectamine® 2000	Thermo Fisher Scientific	Cat# 11668019
Polyethyleneimine	Polysciences	Cat# 23966-2
L-Glutamine (200 mM)	Thermo Fisher Scientific	Cat# 25030081
Fetal Bovine Serum (FBS)	Thermo Fisher Scientific	Cat# 10270106
Trypsin-EDTA (0.05%), phenol red	Thermo Fisher Scientific	Cat# 25300054
Methanol CHROMASOLV, for HPLC, 99,9%	Honeywell	Cat# 34860
Hoechst 33342, 10 mg·mL^{-1} solution	Thermo Fisher Scientific	Cat# H3570
ProLong™ Diamond Antifade Mountant	Thermo Fisher Scientific	Cat# P36961
4-15% Mini-PROTEAN TGX Stain-Free Gels, 10-well	Bio-Rad Laboratories	Cat# 4568083
4-15% Mini-PROTEAN TGX Stain-Free Gels, 15-well	Bio-Rad Laboratories	Cat# 4568086
4-15% Criterion™ TGX Stain-Free Protein Gels, 26 well, 15 μl	Bio-Rad Laboratories	Cat# 5678085
NuPAGE™ 4 to 12%, Bis-Tris, 1.0 mm, Mini Protein Gels, 10 well	Thermo Fisher Scientific	Cat# NP0321BOX
NuPAGE™ 4 to 12%, Bis-Tris, 1.0 mm, Mini Protein Gels, 12 well	Thermo Fisher Scientific	Cat# NP0322BOX
NuPAGE™ 4 to 12%, Bis-Tris, 1.0 mm, Mini Protein Gels, 15 well	Thermo Fisher Scientific	Cat# NP0323BOX

(*Continued on next page*)

Continued

REAGENT or RESOURCE	SOURCE	IDENTIFIER
mPAGE® 4-12% Bis-Tris Precast Gel, 10 well	Merck KgaA	Cat# MP41G10
mPAGE® 4-12% Bis-Tris Precast Gel, 15 well	Merck KgaA	Cat# MP41G15
4-20% Mini-PROTEAN TGX Stain-Free Gels, 10-well	Bio-Rad Laboratories	Cat# 4568094
4-20% Mini-PROTEAN TGX Stain-Free Gels, 12-well	Bio-Rad Laboratories	Cat# 4568095
4-20% Mini-PROTEAN TGX Stain-Free Gels, 15-well	Bio-Rad Laboratories	Cat# 4568096
NuPAGE LDS Sample Buffer (4X)	Thermo Fisher Scientific	Cat# NP0008
Protein Sample Loading Buffer (4X)	LI-COR	Cat# 928-40004
Bromophenol blue sodium salt	Merck KgaA	Cat# B5525
PageRuler™ Prestained Protein Ladder	Thermo Fisher Scientific	Cat# 26617
PageRuler™ Plus Prestained Protein Ladder	Thermo Fisher Scientific	Cat# 26620
InstantBlue, 1 L Protein Stain	Biozol	Cat# EXP-ISB01L
Trans-Blot Turbo RTA Mini 0.2 μm Nitrocellulose Transfer Kit	Bio-Rad Laboratories	Cat# 1704270
Trans-Blot Turbo RTA Midi 0.2 μm Nitrocellulose Transfer Kit	Bio-Rad Laboratories	Cat# 1704271
Milk powder, skim milk	Merck KgaA	Cat# 70166
Amersham ECL Select Western Blotting Detection Reagent	Cytiva	Cat# RPN2235
Amersham ECL Prime Western Blotting Detection Reagent	Cytiva	Cat# RPN2236
Ponceau S	Merck KgaA	Cat# P3504
Critical commercial assays		
HisTrap™ High Performance 5 mL column	Cytiva	Cat# 17-5248-02
BabyBio Ni-IDA 5 mL column	Bio-Works	Cat# 45655007
GSTrap™ 4B 5 mL column	Cytiva	Cat# 28-4017-48
PureCube Compact Cartridge HiCap StrepTactin 1 mL	Cube Biotech	Cat# 34302
Resource S, 6 mL column	Cytiva	Cat# 17-1180-01
HiTrap Q SP 5 mL column	Cytiva	Cat# 17-1154-01
Superdex® 75 10/300 GL column	Cytiva	Cat# 17-5174-01
Superdex® 75 Increase 10/300 GL column	Cytiva	Cat# 29-1487-21
HiLoad® 16/600 Superdex® 75 pg	Cytiva	Cat# 28-9893-33
Superdex® 200 10/300 GL column	Cytiva	Cat# 17-5175-01
Superdex® 200 Increase 10/300 GL column	Cytiva	Cat# 28-9909-44
HiLoad® 16/600 Superdex® 200 pg	Cytiva	Cat# 28-9893-35
Disposable PD-10 desalting columns	Cytiva	Cat# 17-0851-01
NAP-5 desalting colums	Cytiva	Cat# 17-0853-02
Vivaspin 6 concentrators, 3.000, 10.000 & 30.000 MWCO, PES	Sartorius	Cat# VS0692 Cat# VS0602 Cat# VS0621
Vivaspin 20 concentrators, 3.000, 10.000 & 30.000 MWCO, PES	Sartorius	Cat# VS2091 Cat# VS2002 Cat# VS2021
Amicon Ultra-0.5 Centrifugal Filter Unit 3 kDa	Merck KgaA	Cat# UFC5003

(*Continued on next page*)

Continued

REAGENT or RESOURCE	SOURCE	IDENTIFIER
Amicon Ultra-4 3K and 10K	Merck KgaA	Cat# UFC8003 Cat# UFC8010
Amicon Ultra-15 3K and 10K	Merck KgaA	Cat# UFC9003 Cat# UFC9010
Pierce™ BCA Protein Assay Kit	Thermo Fisher Scientific	Cat# 23225
Deposited data		
Mass spectrometry proteomics data	This paper	PRIDE: PXD045662
Experimental models: Cell lines		
HEK293T	Merck KgaA	Cat# 12022001-1VL; RRID:CVCL_0063
HeLa EGFR knockout	Sara Sigismund	N/A
Sf9 cells	Thermo Fisher Scientific	Cat# 12659017
Experimental models: Organisms/strains		
S. cerevisiae: strain background DF5	Finley et al.[78]	N/A
S. cerevisiae: other strains, see Table S1	This paper	N/A
Oligonucleotides		
Primers, see Table S3	This paper	N/A
siRNA Silencer® Select for human UBE2N, assay ID: s14596	Thermo Fisher Scientific	Cat# 4392420
Recombinant DNA		
Plasmids, see Table S2	This paper	N/A
Software and algorithms		
Image Studio™ version 3.1	LI-COR	N/A
FusionCapt Advance version 17.03	Vilbert-Lourmat	N/A
Image Lab™ Touch Software version 2.3.0.07	Bio-Rad Laboratories	N/A
VisiScope 5-Elements	Visitron Systems GmbH	N/A
MetaVue acquisition software version 7.8.10.0	Molecular Devices	N/A
ImageJ	NIH	N/A
Prism 8	GraphPad	N/A
MaxQuant version 2.1.3.0	Cox and Mann[79]	N/A
R version 4.3.0	R Foundation for Statistical Computing	N/A
limma package version 3.56.1	Bioconductor, Phipson et al.[80]	N/A
Other		
Protein purification protocols, see Methods S1	This paper	N/A

RESOURCE AVAILABILITY

Lead contact

Further information and requests for resources and reagents should be directed to and will be fulfilled by the lead contact, Helle D. Ulrich (h.ulrich@imb-mainz.de).

Materials availability

All unique/stable reagents generated in this study are available from the lead contact upon request. Plasmids designed for the use of the Ubiquiton system have been deposited on Addgene with accession numbers 212711–212822.

Data and code availability

- The mass spectrometry proteomics data have been deposited to the ProteomeXchange Consortium via the PRIDE[81] partner repository with the dataset identifier PXD045662. A list of all diGly-modified sites detected in the human samples is also available as an Excel Table (Table S4).
- This paper does not report original code.
- Any additional information required to reanalyze the data reported in this paper is available from the lead contact upon request.

EXPERIMENTAL MODEL AND STUDY PARTICIPANT DETAILS

All *Saccharomyces cerevisiae* strains used in this study are derivatives of DF5[78] and are listed in Table S1. Yeast cultures were grown at 30°C in media specified in the individual experimental sections. Experiments with human cell lines were performed in HEK293T cells (female) or HeLa EGFR knockout cells (female) as indicated. They were cultured in Dulbecco's Modified Eagle Medium (DMEM) supplemented with 10% fetal bovine serum (FBS), 1% (2 mM) L-glutamine, and 100 $\mu g \cdot mL^{-1}$ penicillin-streptomycin at 37°C with 5% CO_2.

METHOD DETAILS

Antibodies

All antibodies used in this study are listed in the key resources table. Mouse monoclonal anti-GFP antibody (clones 7.1/13.1) was used for detection of GFP *in vitro* and in budding yeast experiments. For the analysis of EGFR* endocytosis in human cells, a rabbit polyclonal anti-GFP antibody was used. Selection of ubiquitin-specific antibodies suitable for the various applications was guided by published data regarding linkage preferences[82] and the recognition of either the N- (clone P4D1) or the C-terminal half (clone #1002A) of ubiquitin. The M1-linkage-specific antibody, LUB9, also recognizes the N-terminal part of ubiquitin and thus the NUbo-tag, but not the N-terminally blocked His_7-NUbo-tag (Figures 1H, 2C, 2D, 3A, and S7F). In our hands, the monoclonal anti-ubiquitin antibody, clone #1002A, exhibited no marked preference for either M1-, K48-, or K63-linkages. The monoclonal anti-ubiquitin antibody, FK2, does not recognize either of the two ubiquitin halves, likely as a result of its selection process.[83] Antibodies against the FRB domain of human mTOR and human FKBP12 were used for detection of the NUbo- and CUbo-modules, respectively.

Plasmid construction

Plasmids used in this study are listed in Table S2. Constructs for recombinant protein production were generated as fusions to a GST- or His_6-tag for purification. Point mutations were introduced by site-directed mutagenesis using PfuTurbo DNA polymerase and verified by sequencing. All constructs containing the CUb motif carry a G76V mutation to prevent cleavage by DUBs in cells.

Ubo-E3s for use in yeast were cloned with the relevant tags under control of the constitutive, strong *ADH1* promoter in integrative vectors, except for assays using GFP as a substrate, where ^{NUbo}VSV and ^{NUbo}E3(63)^{VSV} were expressed under control of the *CUP1* promoter. The sequence of E3(1) was codon-optimized for expression in yeast. Constructs for yeast expression of GFP substrates were placed under control of the *CUP1* promoter in integrative vectors. Plasmids for C-terminal tagging of endogenous yeast substrates with CUbo-GFP or CUbo-AID*-GFP were constructed based on pYM25,[84] resulting in seamless addition of the tags. For NUbo-tagging, we constructed suitable cassettes based on the tagging vector pYM-N4[84] by replacing the HphNT1 marker with budding yeast *URA3* and replacing the N-terminal GFP-tag by either the NUbo or the His_7-NUbo module. The resulting constructs afford expression under control of the *CUP1* promoter.

Constructs for transient expression of Ubo-E3s and yeast Ubc7, Ubc13, and Mms2 in human cells were codon-optimized for human expression and cloned under control of the *CMV* promoter in pDEST-3xFLAG (Ubc7) or pcDNA5/FRT/T0 (all others). In addition, a fusion construct of ^{NUbo}E3(48) to yeast Ubc7 with an *in vivo* cleavable P2A peptide inserted between the two open reading frames, ^{NUbo}E3(48)$^{P2A\text{-}3xFLAG}$Ubc7, was generated to allow expression of both proteins from a single construct. For imaging purposes, mCherry was inserted immediately C-terminally of the E3 domains of ^{NUbo}E3(63) and ^{NUbo}E3(48)$^{P2A\text{-}3xFLAG}$Ubc7. EGFR$^{*CUbo\text{-}GFP}$ was cloned by amplifying the extracellular domain and transmembrane region of EGFR from a plasmid, pcDNA3-EGFR-FLAG-Ub, obtained from Simona Polo[47] and fusing it to CUbo-GFP under control of the *CMV*-promoter in pcDNA5/FRT/T0. Expression constructs for Ubo-tagged histone H2B were prepared by amplifying the H2B open reading frame from a plasmid-based cDNA construct obtained from Thomas U. Mayer (pcDNA3.1_F-Hs_H2B-A-mCherry) and inserting it into the pcDNA5/FRT/TO vector backbone containing a CUbo or NUbo tag.

Production of recombinant proteins

Recombinant bovine ubiquitin was purchased from Merck KgaA. ^{His6}E3(1)$^{CUbo\text{-}Str}$ (carrying a C-terminal TwinStrep-tag) was produced in insect cells. All other recombinant proteins were produced in *Escherichia coli*. Detailed expression and purification conditions, including buffers, for all recombinant proteins can be found in Methods S1. Untagged ubiquitin variants were purified by acid and heat precipitation followed by ion exchange and size exclusion chromatography (SEC).[21,85] ^{Myc}ubiquitin was purified by acid and heat precipitation followed by SEC. ^{GST}Ubc13 was purified on glutathione Sepharose followed by SEC.[77] Murine ^{His6}Uba1 was

purified by immobilized metal affinity chromatography (IMAC) followed by ion exchange and SEC.[86] ^{His6}Ubc13,[21] ^{His6}UBCH7, and ^{MBP}Ubc7^{His6} were purified by IMAC followed by SEC. Mms2 and OTULIN were purified as His_6-TEV-fusions by IMAC followed by cleavage of the His_6-tag by ^{His6}TEV protease, reverse IMAC and SEC.[21,29] PIP-E3(63) was purified as a GST-fusion on glutathione Sepharose followed by Thrombin cleavage of the GST-tag, reverse GSTrap and SEC.[18] OTUB1 and AMSH were purified as GST-3C-fusions by GSTrap chromatography followed by cleavage of the GST-tag by ^{GST}PreScission protease, reverse GSTrap and SEC.[29]

NUbo-fusion proteins were lysed in IMAC A buffer supplemented with SIGMAFAST protease inhibitor cocktail, 1 mM DTT and 0.1% Triton X-100 by sonication (Branson Sonifier 450) and subjected to IMAC followed by SEC. CUbo-fusion proteins, which are prone to solubility problems, were lysed in IMAC A supplemented with 1 mM DTT by two passes through a high-pressure cell disruptor (Constant Systems) in continuous flow at 4°C. After lysis, SIGMAFAST protease inhibitor cocktail, 0.1% Triton X-100, 1 mM $MgCl_2$ and 50 U·mL^{-1} SmNuclease were added, followed by an incubation for 20 min at 4°C. The cleared supernatant was subjected to IMAC followed by SEC.

^{His6}E3(1)$^{CUbo\text{-}Str}$ was expressed in SF9 insect cells for 50 h at a density of 9·10^5 cells·mL^{-1} in SF900-III medium using the Bac-to-Bac Baculovirus expression system (Thermo Fisher Scientific). Cells were resuspended in IMAC A SF9 supplemented with 1 mM $MgCl_2$, 1 mM TCEP, 0.2% Triton X-100, cOmplete™ EDTA-free protease inhibitor cocktail and 100 U·mL^{-1} SmNuclease and lysed by brief sonication. The cleared lysate was applied to a Ni-IDA column, using an automated chromatography system (Biorad NGC Quest Plus). After extensive washing with IMAC A and IMAC A supplemented with 35 mM imidazole, the E3 was eluted by applying a linear gradient to 100% IMAC B. Fractions containing ^{His6}E3(1)$^{CUbo\text{-}Str}$ were pooled and loaded onto a StrepTactin 1 mL column. After washing with StrepTactin A buffer, bound protein was eluted using StrepTactin B buffer. Eluted ^{His6}E3(1)$^{CUbo\text{-}Str}$ was re-buffered into gel filtration buffer using a PD-10 column (Cytiva). Aliquots were snap-frozen in liquid nitrogen and stored at -80°C.

In vitro ubiquitylation assays

In vitro substrate ubiquitylation assays were carried out in reactions containing 40 mM HEPES, pH 7.4, 50 mM NaCl, 8 mM magnesium acetate, 100 μM ATP, 10 μM ubiquitin, 50 nM ^{His6}Uba1, 0.2 μM (^{His6}UBCH7 and ^{His6}Ubc13·Mms2) or 1 μM (^{MBP}Ubc7^{His6}) E2, 1 μM substrate, 1 μM E3 and 5 μM rapamycin. Reactions were incubated at 30°C (^{NUbo}E3(48)^{His6} and ^{NUbo}E3(63)^{His6}) or 37°C (^{His6}E3(1)$^{CUbo\text{-}Str}$) for the indicated times, terminated by addition of NuPAGE LDS sample buffer with 25 mM DTT, and analyzed by SDS-polyacrylamide gel electrophoresis (PAGE) and western blotting using the indicated antibodies. Initial assays with PCNA as a substrate were performed with ^{GST}Ubc13 instead of ^{His6}Ubc13 and 5 μM instead of 10 μM ubiquitin.

Yeast strain construction

Oligonucleotides used for genetic manipulations are listed in Table S3. Gene deletions, promoter replacements and gene tagging were introduced by PCR-based methods.[84] To render budding yeast insensitive to rapamycin, we integrated the *TOR1-1* (S1972R) allele, amplified by PCR from TB50 (*TOR1-1 TOR2-1*) genomic DNA, into the DF5 strain background and then deleted *FPR1*.[25]

Ubiquiton model substrates and Ubo-E3s were integrated into the *LEU2* or *URA3* locus. Except for assays involving Cdc45, Ask1, and Cdc11 and initial Hxt3 localization studies, Ubo-E3s were paired with their substrates by mating and diploids were used for subsequent assays. N-terminal tagging of Hxt3 under control of its endogenous promoter was carried out by integration of PCR cassettes *URA3-pCUP1-NUbo* or *URA3-pCUP1-His$_7$-NUbo* and subsequent replacement of the *URA3-pCUP1* module with the *HXT3* promoter, amplified by PCR from genomic DF5 DNA with suitable 45 bp overhangs, via selection on 5-FOA plates (synthetic complete with 0.032 mg·mL^{-1} uracil, 0.032 mg·mL^{-1} adenine, 2% glucose, and 1 mg·mL^{-1} 5-fluoroorotic acid). Plasmids for expression of *Arabidopsis thaliana AFB2* were integrated into the *TRP1* locus.

Ubiquitylation and degradation assays in yeast

For substrate ubiquitylation assays in budding yeast, a saturated culture of yeast cells grown overnight in synthetic complete medium containing 2% glucose (SCG) was diluted to an OD_{600} of 0.2 in SCG medium containing 100 μM $CuSO_4$ and grown to an OD_{600} of ~1. If not stated otherwise, 2 μM rapamycin were added from a 5 mM stock solution in DMSO and samples of 1 OD_{600} unit were collected at the indicated time points and flash-frozen using dry ice. Whole cell extracts were prepared by trichloroacetic acid (TCA) precipitation as described,[21] denatured in NuPage LDS sample buffer supplemented with 50 mM Tris-HCl pH 8.0 and 25 mM DTT for 15 min at 65°C, and analyzed by SDS-PAGE followed by western blotting with the indicated antibodies. Western blots were imaged with an Odyssey® CLx or Odyssey® M system (LI-COR) using near-infrared fluorophore-labelled secondary antibodies.

Degradation assays were performed as above with the following modifications: 1. cultures were grown in yeast extract-peptone-dextrose (YPD) medium if not stated otherwise; 2. before addition of rapamycin, CHX was added at 100 μg·mL^{-1}; 3. fixed volumes equaling 1 OD_{600} unit were collected at t=0 and flash-frozen. To inhibit proteasomal activity, 50 μM MG132 were added 60 min before addition of CHX and rapamycin where indicated. For comparison to the AID* technology, auxin was used at 500 μM.

Denaturing Ni-NTA pull-down from yeast

Yeast cells were diluted in SCG medium supplemented with 100 μM $CuSO_4$ and 2 μM rapamycin to an OD_{600} of 0.0025 and incubated for ~18 h. For the detection of substrate modifications, 140 OD_{600} units were collected and subjected to denaturing affinity

purification using Ni-NTA agarose beads as described.[87] Samples were eluted from the beads by incubation at 65°C for 10 min in NuPage LDS sample buffer supplemented with 25 mM DTT and analyzed by SDS-PAGE and western blotting with the indicated antibodies.

UbiCRest assays

UbiCRest assays[29] were performed on total lysates of yeast cells treated with 2 μM rapamycin for 3 h. Lysates were prepared in a lysis buffer (50 mM Tris, 140 mM NaCl, 15 mM imidazole, pH 8.0) supplemented with 0.1% Triton X-100, 10 mM N-ethylmaleimide (NEM) and SIGMAFAST protease inhibitor cocktail by bead beating with 0.5 mm Zirconia/glass beads (Carl Roth) using a Precellys Evolution (2 mL tubes, 6,800 rpm, 10x 20 s, pause: 60 s, Cryolys set to 4°C, Bertin Technologies). After bead beating, 0.9% Triton X-100, 0.1% SDS, 0.5% sodium deoxycholate, 2 mM $MgCl_2$ and 50 U·mL^{-1} SmNuclease were added and samples were incubated on a roller at 4°C for 15 min. Lysates were cleared by centrifugation at 21,100*g* for 20 min at 4°C. Ni-NTA agarose beads were added to the cleared lysates and samples were incubated on a roller for 60 min at 4°C. Beads were washed three times with wash buffer (50 mM Tris, 140 mM NaCl, 15 mM imidazole, 0.5% Triton X-100, 0.05% SDS, 0.25% sodium deoxycholate, pH 8.0) followed by three washes with DUB reaction buffer (50 mM Tris, 50 mM NaCl, 5 mM DTT, pH 7.5). DUBs (1 μM USP2cc, 1 μM OTULIN, 20 μM OTUB1, or 5 μM AMSH) in a total of volume of 80 μL in DUB reaction buffer were added and beads were incubated at 37°C for 60 min while shaking at 1,200 rpm in a thermomixer (Eppendorf). After addition of 2x NuPage LDS sample buffer supplemented with 50 mM DTT, samples were incubated at 95°C for 10 min and analyzed by SDS-PAGE and western blotting with the indicated antibodies.

Mass spectrometry (yeast)

SILAC experiments were performed for each linkage in triplicates in diploid *lys1Δ* cells expressing combinations of Ubo-enzymes and substrates [M1: ^{myc}E3(1)$^{CUbo\text{-}VSV}$ with ^{NUbo}GFP^{His6} or $^{His7\text{-}NUbo}$GFP; K48: ^{NUbo}E3(48)^{VSV} with $^{His6\text{-}CUbo}$GFP or $^{His6\text{-}CUbo(K48R)}$GFP and overexpression of *UBC7*; K63: ^{NUbo}E3(63)^{VSV} with $^{His6\text{-}CUbo}$GFP or $^{His6\text{-}CUbo(K63R)}$GFP and overexpression of *UBC13* and *MMS2*]. Cells were grown and treated as described for standard *in vivo* ubiquitylation assays, except that cultures were pre-grown twice overnight by dilution into fresh batches of synthetic complete SILAC medium [SCG SILAC, containing 2% glucose, 15 mg·L^{-1} of L-arginine, and 30 mg·L^{-1} of L-lysine-0 ('light'), L-lysine-4 ('medium'), or L-lysine-8 ('heavy')] before induction of the substrates with $CuSO_4$ and finally activation of ubiquitylation by rapamycin treatment for 3 h. Conditions were as follows: 'light' – functional Ubo without rapamycin; 'medium' – Ubo acceptor site mutants with rapamycin; 'heavy' – functional Ubo with rapamycin. For each linkage, samples corresponding to 'light'-, 'medium'-, and 'heavy'-labeled cells (100 OD_{600} units each) were pooled and subjected to denaturing Ni-NTA pull-down as described[87] with the following modifications: cell pellets were resuspended in 25 mL of ice-cold water and volumes scaled accordingly. TCA precipitates were resuspended in 6 mL Buffer A (6 M guanidine HCl, 100 mM sodium phosphate, pH 8.0, 10 mM Tris–HCl, pH 8.0), and 150 μL of Ni-NTA agarose slurry per experiment were incubated with the lysates for 1 h at room temperature. Before elution, beads were additionally washed three times with 1 mL of PBS + 0.05% Tween 20. Bound material was eluted in 100 μL of 50 mM Tris-HCl, pH 8.0, with 0.5% SDS at 65°C for 15 min, followed by a second elution with 50 μL of the same buffer. Combined elutions were flash-frozen using dry ice. For label-free proteomics analysis of the M1-Ubiquiton, diploid cells were grown in standard SCG medium as described for standard *in vivo* ubiquitylation assays in a single overnight culture in three independent replicates. For each condition, 300 OD_{600} units were subjected to denaturing Ni-NTA pull-downs as above. All yeast pull-down samples were processed using the SP3 method.[88] Proteins were then digested using trypsin overnight at 37°C. The resultant peptide solution was purified by solid phase extraction in C_{18} StageTips.[89]

Peptides were analyzed using an Orbitrap Exploris 480 mass spectrometer (Thermo Fisher Scientific) coupled to EASY-nLC 1200 UHPLC system (Thermo Fisher Scientific). Peptides were separated in an in-house packed 60-cm analytical column (inner diameter: 75 μm; ReproSil-Pur 120 C_{18}-AQ 1.9-μm silica particles, Dr. Maisch GmbH) by online reversed phase chromatography through a 90-min gradient of 2.4-32% acetonitrile with 0.1% formic acid at a nanoflow rate of 250 nL/min. The eluted peptides were sprayed directly by electrospray ionization into the mass spectrometer. Mass spectrometry measurement was conducted in data-dependent acquisition mode using a top15 method with one full scan (resolution: 60,000, scan range: 300-1,650 m/z, target value: 3×10^6, maximum injection time: 28 ms) followed by 15 fragmentation scans via higher energy collision dissociation (HCD; normalised collision energy 30%; resolution: 15,000, target value: 1×10^5, maximum injection time: 40 ms, isolation window: 1.4 m/z). Only precursor ions of +2 to +6 charge state were selected for fragmentation scans. Additionally, precursor ions already isolated for fragmentation were dynamically excluded for 25 s.

Mass spectrometry data processing (yeast)

Mass spectrometry raw data files were processed using MaxQuant software (version 2.1.3.0).[79] MS/MS mass spectra were searched using Andromeda search engine[90] against a target-decoy database containing the forward and reverse protein sequences of UniProt *S. cerevisiae* reference proteome release 2022_03 (6,089 entries), together with the protein sequences of the corresponding transgenic proteins and a default list of common contaminants. Trypsin/P specificity was assigned. Methionine oxidation, protein N-terminal acetylation, carbamidomethylation of cysteine, NEM-derivatized cysteine and diGly remnant at lysine residue were chosen as variable modifications. A maximum of 2 missed cleavages were tolerated. The minimum peptide length was set to be 7 amino acids. When applicable, corresponding SILAC labels were included. False discovery rate (FDR) was set to 1% at both peptide and protein levels.

For the SILAC data, the normalized ratios of the detected diGly (K) sites were log_2-transformed (when applicable, ratios of a label-swap replicate were first inverted). The diGly (K) sites of ubiquitin were then used for linkage type analysis. For the label-free pull-down data, the intensities of peptide evidences associated with each detected diGly (K) site were summed and then normalized according to the overall detected peptide intensities in each sample, assuming the overall peptide intensities were similar across the test conditions. These normalized summed intensities of diGly (K) sites were then used for linkage type analysis, with the exception of the M1 linkage, since that corresponds to a linear, not a branched peptide. We therefore used the peptide corresponding to the linear junction between ubiquitin monomers within yeast Ubi4 to assess the M1-linkage. The summed peptide intensities of each linkage type were then log_2-transformed and used for calculating the mean ratio comparing the different test conditions.

Yeast survival assays

Exponential cultures of yeast strains harboring tagged substrates (GFP, CUbo-GFP, AID*-GFP or CUbo-AID*-GFP) and their respective control strains in YPD medium were spotted in five-fold serial dilutions, starting with an OD_{600} of 0.2, onto freshly prepared YPD agar plates containing either DMSO or 2 μM rapamycin in DMSO or 500 μM auxin. Plates were imaged after incubation for two days.

Analysis of Hxt3 endocytosis

Cells were grown to logarithmic phase in DO-HIS medium [CSM-His (MP Biomedicals), Yeast Nitrogen Base (Difco) and 2% glucose (Merck KgaA)]. After addition of 1.1 μM rapamycin, cells were incubated for the indicated times.

For analysis by western blot, 1 mL of cell suspension was precipitated with 10% trichloroacetic acid (TCA) for 10 min on ice. Cells were lysed by bead beating in 10% TCA for 10 min. After centrifugation, the pellet was resuspended in TCA sample buffer (50 mM Tris-HCl, pH 6.8, 100 mM dithiothreitol, 2% SDS, 0.1% bromophenol blue, and 10% glycerol containing 200 mM of unbuffered Tris) at a concentration of 50 μL per initial OD_{600} unit. Samples were denatured at 37°C for 10 min and analyzed by SDS-PAGE followed by western blotting with the indicated antibodies. As loading control, total proteins were visualized by in-gel fluorescence using a trihalo compound incorporated in stain-free TGX gels, 4–20% after 45 s UV-induced photoactivation using a ChemiDoc MP imager (BioRad).

For fluorescence microscopy, cells were mounted in DO-HIS medium and imaged at room temperature with a motorized Olympus BX-61 fluorescence microscope equipped with an Olympus PlanApo 100x oil-immersion objective (1.40 NA), a QiClick cooled monochrome camera (QImaging, Surrey, BC, Canada), and the MetaVue acquisition software. GFP-tagged proteins were visualized using a GFP filter set (41020 from Chroma Technology, Bellows Falls, VT; excitation HQ480/20x, dichroic Q505LP, emission HQ535/50m). Images were analyzed and processed in ImageJ.

Analysis of Hxt3 ubiquitylation

Yeast cultures were grown to an OD_{600} of ~1 in SCG medium. After collection of a sample of 50 OD_{600} units (t=0), 2 μM rapamycin were added, followed by incubation for 30 min with shaking and collection of another sample of 50 OD_{600} units. Cells were lysed in 460 μL of GFP-trap lysis buffer (50 mM HEPES pH 7.5, 1 mM EDTA pH 8.0, 140 mM NaCl, 1% glycerol, 0.1% Triton X-100, 20 mM NEM and SIGMAFAST protease inhibitor cocktail) by bead beating with 0.5 mm Zirconia/glass beads using a Precellys Evolution (2 mL tubes, 6800 rpm, 10x 20 s, pause: 60 s, Cryolys set to 4°C, Bertin Technologies). Subsequently, samples were partially denatured by addition of 0.9% Triton X-100, 0.1% SDS, and 0.5% sodium deoxycholate and incubation on a roller at 4°C for 15 min. 600 μL of wash buffer (50 mM HEPES pH 7.5, 140 mM NaCl, 5% glycerol, 1% Triton X-100) supplemented with 20 mM NEM were added, samples were mixed by vortexing, incubated on a roller at 4°C for 30 min and cleared by centrifugation at 10,000*g* at 4°C for 10 min. 20 μL of magnetic agarose GFP binder beads were added to the cleared supernatant and samples were incubated on a roller at 4°C for 45-60 min. Beads were washed twice on a roller with wash buffer at 4°C for 15 min and once with PBS (137 mM NaCl, 2.7 mM KCl, 10 mM Na_2HPO4, 1.8 mM KH_2PO_4) supplemented with 0.1% Tween 20 for 30 min at room temperature. For elution, 25 μL of 2x urea sample buffer (150 mM Tris-HCl, pH 6.8, 6 M urea, 6% SDS, 0.1% bromophenol blue) were added to the beads. After incubation at 37°C for 30 min while shaking at 1,400 rpm, 25 μL of heating buffer (50 mM Tris pH 7.5, 1 mM EDTA, 1% SDS, 20% glycerol) were added, followed by another incubation at 37°C and 1,400 rpm for 30 min. Samples were separated by SDS-PAGE and analyzed by western blotting with the indicated antibodies.

Transfection of human cell lines

For transfection of HeLa EGFR knockout cells, 5 μg of total DNA (equimolar amounts for each construct) per $5 \cdot 10^6$ cells were transfected using Lipofectamine according to the manufacturer's instructions. For transfection of HEK293T cells, 12 μg of total DNA per $5 \cdot 10^6$ cells were mixed with 40 μL of 1 $mg \cdot mL^{-1}$ polyethyleneimine in 2 mL of serum-free DMEM, incubated for 10 min at room temperature, diluted with 6 mL of DMEM with all supplements, and added to cells. For the co-transfection of multiple constructs, plasmids were used in equal mass quantities, except in the following situations: to balance expression levels, the amount of DNA transfected for expression of $EGFR^{*FKBP\text{-}GFP}$ was reduced 5-fold relative to $EGFR^{*CUbo}$ and the amount for expression of $^{Ub*V\text{-}FRB}mCherry^{FLAG}$ was increased 10-fold relative to $^{NUbo}mCherry^{FLAG}$. Cells were harvested for analysis after 24 h.

Preparation of human cell lysates

Cells were rinsed twice with PBS and collected in an Eppendorf tube, centrifuged at 500*g* for 5 min, and the supernatant was aspirated. Cells were lysed in RIPA buffer (50 mM Tris-HCl, pH 7.4, 1 mM EDTA, 1% Triton X-100, 0.5% sodium deoxycholate, 0.1% SDS,

150 mM NaCl, 2.5 mM $MgCl_2$) supplemented with cOmplete™ protease inhibitor cocktail, 10 mM NEM, 1 mM phenylmethanesulfonyl fluoride (PMSF), and 0.5 μl·mL^{-1} SmNuclease, and subjected to brief sonication. Samples were centrifuged at 21,583*g* for 20 min, and the supernatant was transferred to a new pre-cooled tube. Protein concentration was normalized using the Pierce™ BCA Protein Assay Kit, and samples were supplemented with 4x NuPAGE LDS sample buffer and heated at 95°C for 5 min. Proteins were analyzed by SDS-PAGE and western blotting using semi-dry transfer unless otherwise noted. HRP-conjugated secondary antibodies were detected with Amersham ECL Prime Western Blotting Detection Reagent and imaged using Fusion FX (Vilber). IRDye-coupled secondary antibodies were imaged using Odyssey® CLx (LI-COR).

Analysis of H2B polyubiquitylation

$5 \cdot 10^6$ HEK 293T cells were transfected with relevant Ubo-tagged constructs and cultured for 24 h before harvesting. For the M1-Ubiquiton, cells were lysed in RIPA buffer immediately after harvesting, followed by SDS-PAGE and western blot analysis of the lysates. For the K48- and K63-Ubiquiton, 10% of each cell pellet were used for the preparation of total cell extracts and 90% for denaturing Ni-NTA pull-down. For the pull-down, cell pellets were lysed in 1.5 mL Gua-HCl buffer (6 M guanidinium-HCl, 50 mM NaH_2PO_4, 50 mM Na_2HPO_4, 10 mM Tris-HCl pH 8.0, 0.1% Tween 20) and briefly sonicated to reduce the viscosity. Imidazole was added to a final concentration of 15 mM, followed by 40 μL of a 50% Ni-NTA slurry per sample. Lysates were incubated with beads at 4°C overnight with agitation, washed twice with 1 mL of Gua-HCl buffer and four times with 1 mL of urea buffer (8M Urea, 80 mM NaH_2PO_4, 20 mM Na_2HPO_4, 10 mM Tris-HCl pH 6.3, 0.1% Tween 20) each. Proteins were eluted in 50 μL of elution buffer (2x LDS, 200 mM imidazole) at 95°C for 10 min and analyzed by western blotting using the indicated antibodies.

Mass spectrometry (human cells)

HEK 293T cells were cultured for 2 weeks in 'light' (L-arginine-0, L-lysine-0) and in parallel in 'heavy' (L-arginine-10, L-lysine-8) DMEM medium. For each transfection, $15 \cdot 10^6$ cells were plated on 15 cm dishes 24 h prior to transfection. Cells were transfected with polyethyleneimine as described above. Each experiment was performed in triplicate: for two replicates, Ubo-E3s were transfected into 'heavy' and empty vector into 'light' labeled cells; for the third replicate, labels were switched. 24 h after transfection, cells were collected in 1 mL of ice-cold PBS, centrifuged at 500*g* for 5 min, and lysed in RIPA buffer as described above. Lysates from 'light' and 'heavy' labeled cells were mixed 1:1 (corresponding to 5 mg of protein each), and proteins were precipitated by adding 4 volumes of acetone pre-cooled to -20°C. Trypsin digestion and diGly-remnant immunoprecipitation were performed as described[18] with minor modifications: protein pellets were resolubilized in 8 M urea containing 50 mM ammonium bicarbonate. Following reduction by 5 mM DTT, alkylation by 15 mM chloroacetamide in the dark and quenching by 5 mM DTT, the urea concentration was diluted to 2 M using 50 mM ammonium bicarbonate. Proteins were then digested by trypsin (protein:enzyme ratio of 100:1) at room temperature overnight. Following desalting in C_{18} Sep-Pak columns (Waters), peptides were eluted in 50% acetonitrile. Afterwards, the acetonitrile was evaporated in a centrifugal evaporator. The resultant peptide solution was then adjusted to reach 50 mM MOPS-NaOH (pH 7.2), 10 mM Na_2HPO_4, 50 mM NaCl (1X IAP buffer). Thereafter, the peptides were incubated with PTMScan Ubiquitin Branch Motif (K-ε-GG) Immunoaffinity Beads at 4°C overnight. Following sequential washes in 1X IAP buffer and water, peptides were eluted in 0.15% TFA and desalted in C_{18} StageTips. Peptides were analyzed as described for the yeast samples, with modifications to individual parameters (reversed phase chromatography gradient: 120 min; data-dependent acquisition mode: top20 method; maximum injection time: 40 ms; fragmentation scans via HCD: 20; dynamic exclusion of precursor ions: 30 s).

Mass spectrometry data processing (human cells)

Mass spectrometry raw data files were processed as described for the yeast samples, but using *H. sapiens* UniProt reference proteome release 2022_03 (101,761 entries). To search for potential off-target effects on ubiquitylation, the log_2-transformed ratios were filtered for at least 0.9 of localization probability and detection in at least 2 out of 3 replicates. A linear model was then fitted using the limma package in R[80] to assess the ratios for each site without further adjustment for multiple testing. The log_2-fold change and the significance of the difference were displayed in a volcano plot. Only sites with a minimum log_2-fold change of 1 and a *p* value below 0.01 were considered as being differentially regulated.

Analysis of EGFR* degradation

$0.6 \cdot 10^6$ HeLa EGFR knockout cells per well were seeded in 6-well plates and transiently transfected with relevant constructs as described above. 24 h after transfection, cells were pre-treated with 50 μg·mL^{-1} CHX and 30 μM MG132 or 100 μM chloroquine for 60 min. Samples were collected (t=0) and cells were treated with either DMSO or 1 μM rapamycin from a 10 mM stock in DMSO. Samples were collected again after 60 min and 120 min for processing as described above and analysis by western blotting.

Analysis of EGFR* polybiquitylation

$5 \cdot 10^6$ HeLa EGFR knockout cells were seeded in 10 cm plates and transfected with relevant constructs as described. After 24 h, cells were treated with 1 μM rapamycin in DMSO for 2 h. Cells were lysed in RIPA buffer by sonication and protein concentrations were adjusted to each other. An input sample (2%) was retained, and the remaining lysate was used for immunoprecipitation. For each sample, 50 μL protein G agarose beads were pre-blocked with 0.1% BSA in PBS at 4°C for 1 h, washed, and resuspended in 400 μL of RIPA buffer supplemented with cOmplete™ EDTA-free protease inhibitor cocktail. Anti-EGFR antibody (2 μg per IP)

was bound to the beads at 4°C for 2 h. After washing the beads, 0.5 - 1 mg of cell lysate was added and the suspension was gently agitated at 4°C for 2 h. Beads were then washed at least five times with RIPA buffer and bound material was eluted by adding 2x NuPAGE LDS sample buffer supplemented with 100 mM DTT and heating at 65°C for 10 min. Samples were analyzed by SDS-PAGE, followed by western blotting with wet transfer (100 V, 100 min) and probing with the indicated antibodies.

Immunofluorescence of human cells

Coverslips were placed in 6-well plates. Per well, $0.6 \cdot 10^6$ HeLa EGFR knockout cells were seeded and transiently transfected with relevant constructs as described. 24 h after transfection, cells were treated with either DMSO or 1 μM rapamycin in DMSO for 2 h. Following the treatment, cells were washed twice with PBS and fixed and permeabilized with ice-cold methanol for 10 min. Coverslips were then washed three times with PBS and blocked for 1 h with 3% bovine serum albumin (BSA) in PBS/0.1% Triton X-100. Incubation with primary antibody was overnight at 4°C (anti-LAMP2 conjugated with Alexa Fluor® 647 in a 1:100 dilution, anti-calnexin antibody in a 1:250 dilution), followed by three washes of 5 min each with PBS/0. 1% Triton X-100. For anti-calnexin staining, samples were incubated with secondary antibody (goat anti-Rabbit IgG conjugated with Alexa Fluor® 647 in a 1:1000 dilution) for 1 h at room temperature, followed by 3 washes of 5 min each with PBS/0.1% Triton X-100. Nuclei were stained using Hoechst at a dilution of 1:10,000, followed by three 5 min washing steps with PBS. Coverslips were mounted with ProLong™ Diamond Antifade Mountant. Images were acquired at room temperature using a Visiscope 5-Elements spinning-disk confocal fluorescence microscope (Visitron Systems GmbH, Germany) based on a Nikon Ti-2E stand and a CSU-W1 spinning disk scan head (Yokogawa, Japan) with a 50 μm pinhole disk, controlled by the VisiView software. The microscope was equipped with a ×100/1.49 NA apochromatic oil-immersion objective (CFI Plan Apo SR TIRF, Nikon) and a Prime BSI sCMOS camera (2048 x 2048 pixels, 6.5 μm pixel size, Photometrics). Laser lines of 405 nm, 488 nm, 561 nm and 640 nm were used for the fluorescence excitation and the emission was acquired using filters ET460/50m (Chroma), ET525/50m (Chroma), FF01-623/32 (Semrock) and FF01-692/40 (Semrock) respectively. Images were analyzed with ImageJ.

QUANTIFICATION AND STATISTICAL ANALYSIS

For quantification of linkages in yeast samples, $\log_2$-ratios of summed intensities of diGLy peptides, quantified by mass spectrometry as described, were plotted individually from three replicates and mean values and standard deviations were calculated and indicated on the plots. For quantification of degradation rates, western blot signals were quantified using Image Studio™ Ver. 3.1 (LI-COR). For substrate signals (anti-GFP, 800 channel), shapes of equal size covering both modified and unmodified species were used. A shape of the same size was used for background correction. Tubulin (anti-Tub1, 700 nm channel) served as a loading control. For each sample, total intensities were divided by the respective shape size to calculate signal densities, background signal was subtracted, and the GFP signal was calculated relative to the Tub1 signal. The calculated signal at t=0 in each strain was set to 100%, and subsequent values were calculated relative to this. All calculations were performed in Excel 2016. Mean and standard deviations from three independent biological replicates were calculated and plotted using Prism 8.

ADDITIONAL RESOURCES

Detailed expression and purification conditions, including buffers, for all recombinant proteins can be found in Methods S1.